Ore Geology Reviews 34 (2008) 317–336

Contents lists available at ScienceDirect

Ore Geology Reviews

journal homepage: www.elsevier.com/locate/oregeorev

Mineral chemistry of ore and hydrothermal alteration at the Sossego iron oxide–copper–gold deposit, Carajás Mineral Province, Brazil

Lena Virgínia Soares Monteiro [a,*], Roberto Perez Xavier [a], Murray W. Hitzman [b], Caetano Juliani [c], Carlos Roberto de Souza Filho [a], Emerson de R. Carvalho [a]

[a] Instituto de Geociências, Universidade Estadual de Campinas, R. João Pandiá Calógeras, 51, CEP 13083-970, Campinas, SP, Brazil
[b] Department of Geology and Geological Engineering, Colorado School of Mines, Golden, Colorado 80401, United States
[c] Instituto de Geociências, Universidade de São Paulo, Rua do Lago, 562, CEP 05508-080, São Paulo, SP, Brazil

ARTICLE INFO

Article history:
Received 10 January 2007
Received in revised form 13 October 2007
Accepted 31 January 2008
Available online 3 March 2008

Keywords:
Sossego deposit
Iron oxide–copper–gold deposit
Carajás Mineral Province
Brazil
Mineral chemistry
Geothermobarometry

ABSTRACT

The Sossego iron oxide–copper–gold deposit in the Carajás Mineral Province comprises two major orebodies, Sequeirinho and Sossego. Sodic alteration (albite–hematite) and sodic–calcic alteration zones represented by albite, ferro-edenite/hastingsite (up to 3.8 wt.% Cl), actinolite/magnesiohornblende, magnetite, titanite, epidote, and calcite are predominant at Sequeirinho. Magnetite bodies with envelopes of apatite-rich actinolitite were formed with the sodic–calcic event at high temperatures (~500 °C at 1.4 kbar). In the Sossego orebody, potassic alteration with orthoclase and Cl-rich biotite (up to 3.1 wt.%) and chloritization are the main alteration types.
Mineralized breccias in both orebodies have coarse-grained zoned actinolite/ferro-actinolite, Cl-apatite, and magnetite within the matrix. Sulfides occur in equilibrium with a paragenetically late calcite–quartz–chlorite–epidote–allanite assemblage. The Al^{IV} contents of the chlorite indicate crystallization at temperatures below 300 °C. Chalcopyrite occurs associated with pyrite (up to 2.3 wt.% Co and 0.2 wt.% Ni), native gold (up to 14.9 wt.% Ag), siegenite, millerite, vaesite, Pd-melonite, and hessite.
Dilution and cooling of the hot metalliferous fluid (>500 °C) by mixing with meteoric fluids may have been the main mechanisms responsible for the deposition of metals transported as metal chloride complexes in both orebodies of the Sossego deposit.

1. Introduction

The Carajás Mineral Province, located at the southeast part of the Amazon Craton in Pará State, Brazil, contains the world's largest known concentration of large-tonnage iron oxide–copper–gold (IOCG) deposits, such as Sossego (245 Mt at 1.1 wt.% Cu, 0.28 g/t Au; Lancaster et al., 2000), Salobo (789 Mt at 0.96 wt.% Cu, 0.52 g/t Au, 55 g/t Ag; Souza and Vieira 2000), Cristalino (500 Mt at 1.0 wt.% Cu; 0.3 g/t Au, Huhn et al., 1999), Igarapé Bahia/Alemão (219 Mt at 1.4 wt.% Cu, 0.86 g/t Au; Tallarico et al., 2005), Gameleira (100 Mt at 0.7 wt.% Cu; Rigon et al., 2000), and Alvo 118 (70 Mt at 1.0 wt.% Cu, 0.3 g/t Au; Rigon et al., 2000).

The Sossego mine operated by the Companhia Vale do Rio Doce (CVRD) was the first major IOCG deposit to go into production in Brazil in 2004. This deposit is distinctive because it appears to contain hydrothermal alteration zones similar to those formed at a range of depths in IOCG hydrothermal systems worldwide (Monteiro et al., 2008). The Sossego deposit shares a number of similarities with the other Carajás IOCG deposits, including the occurrence of chlorine-bearing mineral phases and strong enrichment in rare earth elements, Co, Ni, Pd and U (Guimarães, 1987; Zang and Fyfe, 1995; Tavaza et al., 1999; Huhn et al., 1999; Lindenmayer et al., 2001; Dreher, 2004). Cobalt and Ni enrichments, and their association with Cl-rich silicates, have been also recognized as important characteristics of IOCG deposits worldwide (Mazdab et al., 1999; Mazdab and Barton, 2001; Sillitoe, 2003). However, these characteristics are related to the most controversial aspect of the genesis of this deposit class, namely the source of fluids and metals.

Distinct sources for salinity and metals in IOCG deposits have been considered in dominantly magmatic-hydrothermal systems, such as the Cloncurry district, Australia (Rotherham et al., 1998), and the Candelária, Punta del Cobre, Manto Verde, and Cerro Negro IOCG deposits in Chile and Peru (Sillitoe, 2003), in hybrid systems with magmatic-hydrothermal and non-magmatic components (e.g., Emmie Bluff, Australia; Gow et al., 1994; Olympic Dam, Australia; Haynes et al., 1995), and in systems in which a magmatic fluid component is likely absent (e.g., Wernecke Mountains, Yukon, Canada; Hunt et al., 2005). Indeed, a variety of geological processes seem to influence the formation of IOCG systems, explaining the diversity of these systems (Hitzman, 2000).

Systematic studies on the variations of physicochemical parameters (temperature, pressure, redox changes) related to evolution

* Corresponding author. Tel.: +55 19 35214575; fax: +55 19 32891097.
E-mail addresses: lena@ige.unicamp.br (L.V.S. Monteiro), xavier@ige.unicamp.br (R.P. Xavier), mhitzman@mines.edu (M.W. Hitzman), cjuliani@usp.br (C. Juliani), beto@ige.unicamp.br (C.R. de Souza Filho), emersonr@ige.unicamp.br (E.R. Carvalho).

0169-1368/$ – see front matter © 2008 Elsevier B.V. All rights reserved.
doi:10.1016/j.oregeorev.2008.01.003

of the Carajás IOCG deposits are of fundamental importance for the characterization of the processes responsible for the development of the Carajás giant hydrothermal system(s) and ore deposition.

In the Sossego IOCG deposit, detailed petrographic studies permitted outline a consistent paragenetic sequence and the spatial zoning of alteration and mineralization (Monteiro et al., 2008). These studies enable the characterization of mineral chemistry variations during the hydrothermal system evolution. Additionally, this study allows comparison to available information on other IOCG deposits in the Carajás Mineral Province.

2. Geological setting of the Carajás Mineral Province

The Carajás Mineral Province, located in the southern part of the Amazon Craton, is divided into two tectonic blocks, the southern Rio Maria greenstone terrain (Huhn et al., 1988), and the northern Itacaiúnas Shear Belt (Araújo et al., 1988). The oldest units in the province occur in the southern block and encompass the Arco Verde Tonalite (2.97 to 2.90 Ga; Pimentel and Machado, 1994) and the 2.9 Ga Andorinhas Supergroup greenstone belt sequences (Docegeo, 1988; Araújo et al., 1988; Faraco et al., 1996). Within the northern block of the Carajás Mineral Province (Fig. 1), the Archean basement is represented by the Xingu Complex (~2.8 Ga, Machado et al., 1991), composed of tonalitic to trondhjemitic gneiss and migmatites, and by the Pium Complex (~3.0 Ga, Rodrigues et al., 1992; Pidgeon et al., 2000).

The basement rocks are overlain by the Carajás Basin, which comprises the metavolcano-sedimentary sequences of the 2.73–2.76 Ga Itacaiúnas Supergroup (Wirth et al., 1986; Machado et al., 1991; Macambira et al., 1996; Trendall et al., 1998; Galarza and Macambira, 2002a,b; Pimentel et al., 2003; Tallarico et al., 2005). This supergroup encompasses the Igarapé Salobo, Igarapé Pojuca, Grão Pará, and Igarapé Bahia groups (Wirth et al., 1986; Docegeo, 1988), which were variably affected by deformation and metamorphism during the Archean (2.7 to 2.5 Ga; Dardenne and Schobbenhaus, 2001; Galarza and Macambira, 2002a).

The Igarapé Salobo Group, the host to the Salobo IOCG deposit, consists of paragneiss, amphibolites, quartzites, meta-arkoses and iron formations, whereas the Igarapé Pojuca Group (2732±3 Ma, U–Pb

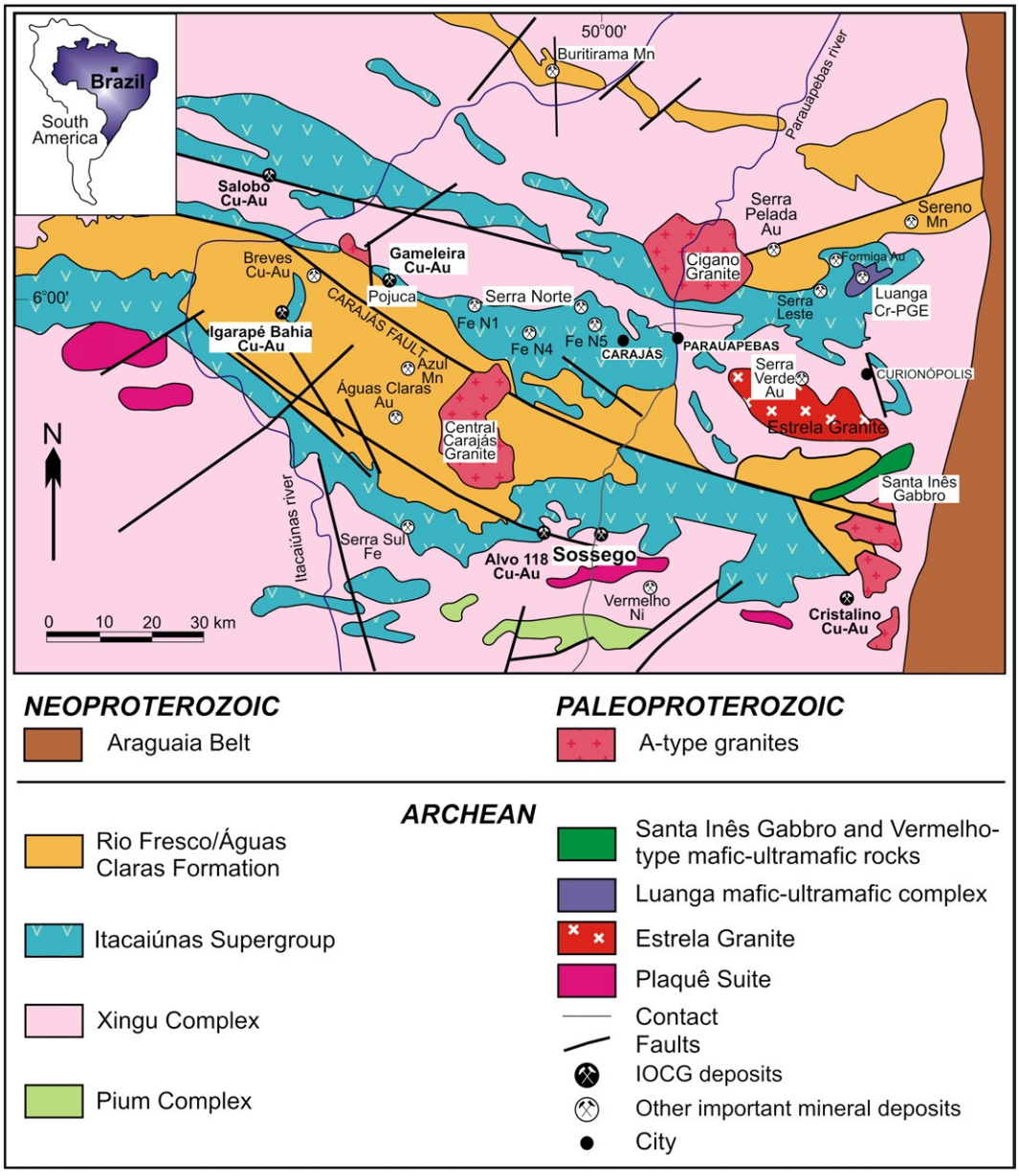

Fig. 1. Simplified geological map of the Carajás Mineral Province (Docegeo, 1988; Dardenne and Schobbenhaus, 2001).

zircon; Machado et al., 1991) contains greenschist to amphibolite facies rocks, represented by basic metavolcanic rocks, pelitic schists and iron formations. The latter hosts both the Pojuca Cu–Zn and Gameleira IOCG deposits (Galarza and Macambira, 2002b). The Grão Pará Group comprises greenschist facies metamorphic units, including metabasalts, felsic metavolcanic rocks, and iron formations that contain outstanding iron deposits. Greenschist facies metavolcanic, metapyroclastic and metasedimentary rocks, including iron formations, define the Igarapé Bahia Group. This hosts the Igarapé Bahia/Alemão IOCG deposit.

The Itacaiúnas Supergroup is overlain by an extensive succession of Archean platform to fluvial sandstones and siltstones, known as the Águas Claras Formation (Nogueira, 1985; Araújo et al., 1988) or the Rio Fresco Group (Docegeo, 1988). This unit covers large areas in the Carajás Mineral Province where it hosts the Azul Mn, the Águas Claras Au, and the Serra Pelada/Serra Leste Au–PGE deposits.

The Itacaiúnas metavolcano-sedimentary sequence is crosscut by 2.76–2.74 Ga syntectonic alkaline granites (Estrela Granite Complex, Plaquê Suite, Planalto and Serra do Rabo; Barros et al., 2001; Dall'Agnol et al., 1997), which produced a tectono-thermal aureole in the metavolcano-sedimentary envelope and wider scale contact metamorphic effects (Barros and Barbey, 1998). Other Archean intrusions comprise the Luanga mafic–ultramafic complex (2763±6 Ma, Machado et al., 1991) and 2.65 to 2.70 Ga gabbro dikes and sills that intercept the Águas Claras Formation (Dias et al., 1996; Mougeot et al., 1996).

Granitoid intrusions coeval with the Carajás and Cinzento transcurrent fault systems (2581 to 2519 Ma; Pinheiro and Holdsworth, 1997), such as the Old Salobo Granite (2573±2 Ma, U–Pb zircon, Machado et al., 1991) and the Itacaiúnas Granite (2560±37 Ma, Pb–Pb zircon, Souza et al., 1996) also occur in the Province.

Paleoproterozoic magmatism, represented by within-plate A-type, alkaline to subalkaline granites (~1.88 Ga Serra dos Carajás, Cigano, Cigano, Pojuca, Young Salobo, Musa, Jamon, Seringa, Velho Guilherme, and Breves granites; Dall'Agnol et al., 1994, 1999; Tallarico et al., 2004) is widespread in the province. Younger alkali-rich leucogranite dikes with a U–Pb SHRIMP age of 1583+9/−7 Ma (Pimentel et al., 2003) are also described in the area of the Gameleira deposit.

The province was also affected by other magmatic events represented by the Borrachudo, Santa Inês and Complexo Lago Grande gabbros (Villas and Santos, 2001) and late diabase dikes, whose ages are uncertain.

3. The Sossego iron oxide–copper–gold deposit

The Sossego deposit (Lancaster et al., 2000) in the Carajás Mineral Province is located along a regional WNW–ESE-striking shear zone that defines the southern contact between metavolcano-sedimentary units of the Itacaiúnas Supergroup and tonalitic to trondhjemitic gneisses and migmatites of the Xingu Complex. This shear zone is crosscut by N- and NW-striking faults and by a dextral system of transcurrent E–W to NE–SW-striking subvertical dipping faults. The latter appears to delineate the mineralized zones at the Sossego deposit (Morais and Alkmim, 2005).

In the Sossego area, granite and granophyric granite are crosscut by gabbro and late dacite porphyry dikes. All these intrusive rocks, whose exact age of emplacement has not been determined, cut the Xingu complex basement and Itacaiúnas metavolcanic rocks, and are form WNW–ESE-trending bodies, concordant with the regional structures. They have been intensely altered by the Sossego hydrothermal system. Late NW-oriented, unaltered diabase dikes crosscut shear zones, faults and all intrusive units.

The Sossego deposit comprises two major groups of orebodies (Fig. 2) with distinct styles and intensities of hydrothermal alteration (Carvalho et al., 2005; Monteiro et al., 2005; Villas et al., 2005). This variability likely reflects both different host rocks and different paleostructural levels (Monteiro et al., 2008). The Sequeirinho orebody represents the bulk of resources, with 85% of the ore reserves. All of the orebodies occur in the hanging wall of major E–W to NE–SW-trending, high angle faults. Rocks in the footwall of the faults are intensely mylonitized metavolcanic rocks that display biotite–tourmaline–marialitic scapolite–(hastingsite) alteration near the fault contact.

Although the type and intensity of alteration and mineralization varies among the different orebodies at Sossego, a consistent paragenetic sequence of alteration and mineralization can be discerned in the system. This paragenetic sequence is mainly represented by early sodic and sodic–calcic alteration accompanied by magnetite±apatite formation (predominant in the Sequeirinho orebody) and potassic alteration, chloritization, calcic, and hydrolytic alteration that predominates within the Sossego orebody (Fig. 3).

3.1. Sequeirinho orebody

The Sequeirinho orebody (Fig. 2) is hosted by granite, gabbro, and felsic metavolcanic rocks that contain minor lenses of metamorphosed ultramafic rocks. These host rocks were strongly affected by both early sodic (chessboard albite–hematite) and fracture-controlled to pervasive sodic–calcic alteration (amphibole–albite–magnetite–calcite–epidote–quartz–titanite–allanite–thorianite). Towards the contact between the gabbro bodies and the granite, both are replaced by sodic–calcic alteration assemblage with ferro-edenite/hastingsite (Fig. 4A, B). This assemblage is overprinted by an actinolitge-bearing

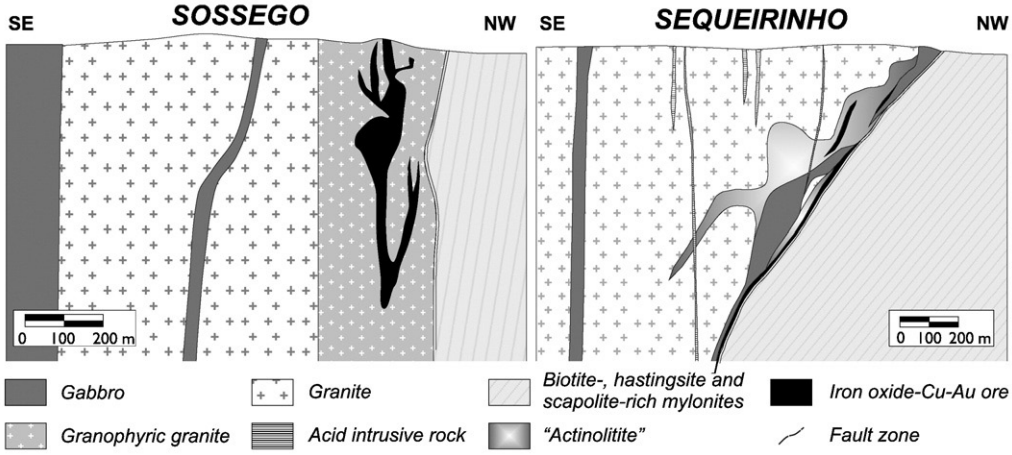

Fig. 2. Simplified cross-section of the Sequeirinho and Sossego orebodies (CVRD).

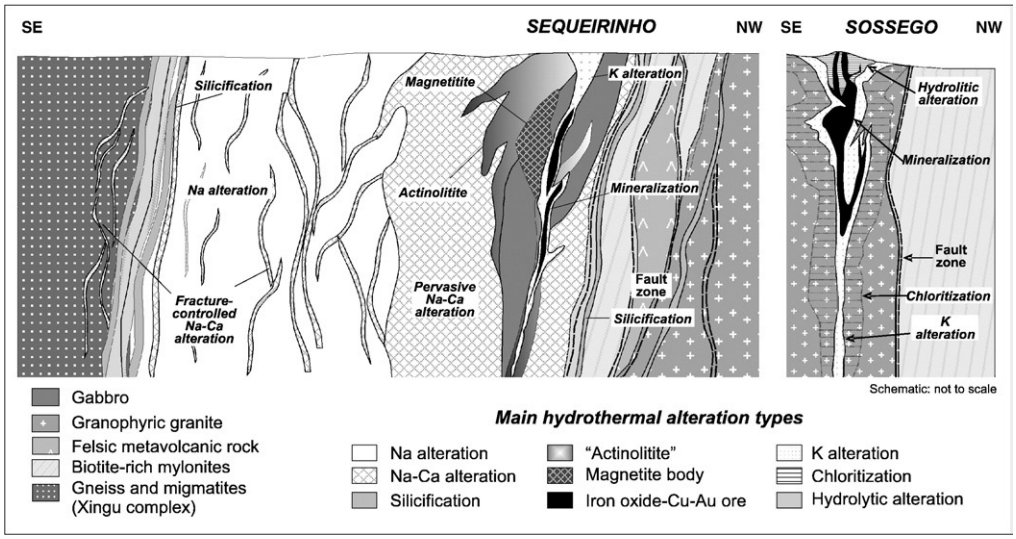

Fig. 3. Schematic profile of the Sequeirinho and Sossego orebodies showing distribution of hydrothermal alteration zones (modified from Monteiro et al., 2008).

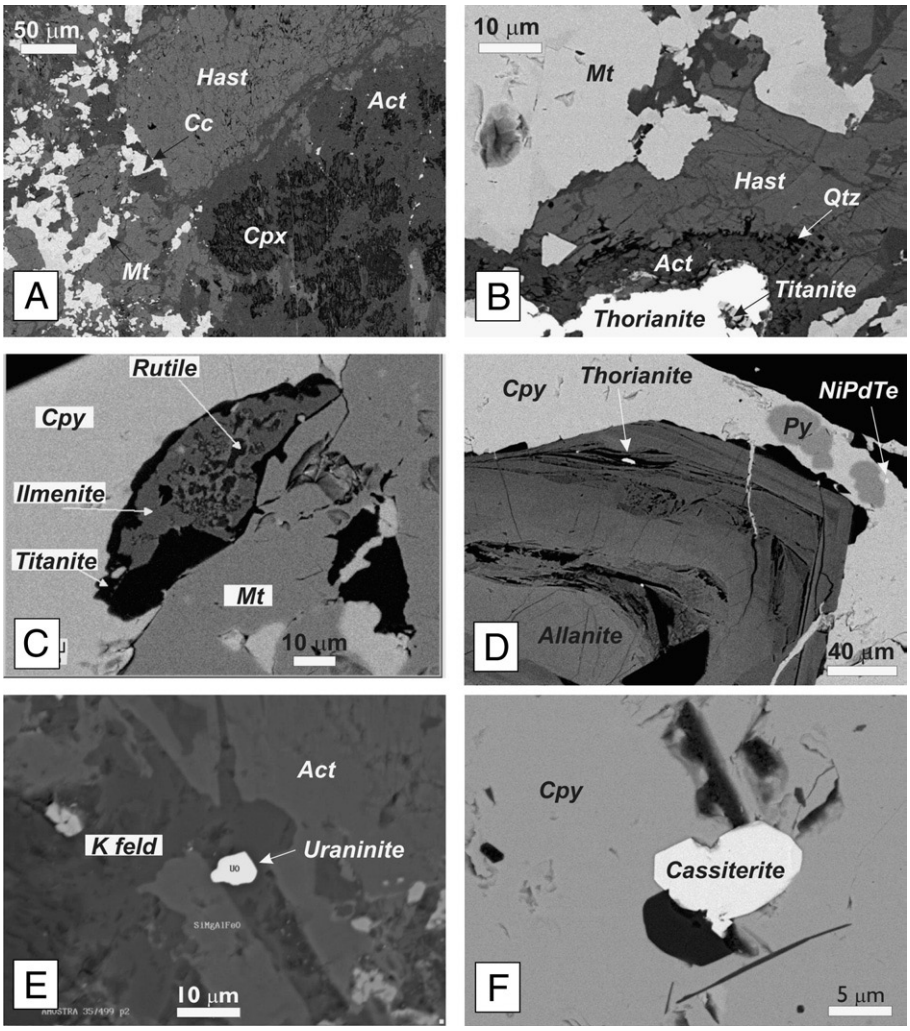

Fig. 4. Back-scattered electron images showing: (A) replacement of igneous clinopyroxene by hastingsite/ferro-edenite–magnetite in gabbro from the Sequeirinho orebody. Actinolite cuts previous hastingsite/ferro-edenite; (B) thorianite associated with actinolite, quartz, and titanite. This assemblage replaces hastingsite/ferro-edenite + magnetite in altered gabbro; (C) Ti-bearing phases associated with magnetite and chalcopyrite in mineralized breccia at Sossego; (D) zoned allanite crystals with thorianite inclusions associated with chalcopyrite and pyrite in the ore breccia from Sequeirinho; (E) uraninite associated with K feldspar (potassic alteration). The latter cuts actinolite (sodic–calcic alteration); (F) cassiterite inclusion in chalcopyrite (Sossego ore). Abbreviations: Act = actinolite; Cc = calcite; Cpx = clinopyroxene; Cpy = chalcopyrite; Hast = hastingsite/ferro-edenite; K feld = potassium feldspar; Mt = magnetite; Py = pyrite; Qtz = quartz.

sodic–calcic assemblage (Fig. 4A, B), which predominates in the Sequeirinho orebody. These sodic–calcic alteration zones are spatially associated with massive magnetite–(apatite) bodies that appear to have replaced gabbro, granite, and felsic metavolcanic rocks. Pervasive sodic–calcic alteration grades into zones of massive, coarse-grained actinolite crystals intergrown with magnetite. This rock type, termed "actinolitite", forms envelopes around massive magnetite bodies and contains apatite-rich bodies, characterized by rose-colored, up to 10 cm-long chlorine-rich apatite crystals.

Magnetite forms subvertical bodies generally parallel to the fault bounding the orebody (Fig. 3). The magnetite crystals are commonly fractured or brecciated and cut by veins with apatite–quartz and calcite–chlorite–quartz–pyrite–chalcopyrite–titanite–rutile–pyrophanite–perovskite associations. The massive magnetite bodies are cut by narrow zones (<30 cm) of poorly developed potassic alteration (K feldspar–biotite–magnetite–quartz–allanite–uraninite–thorianite) that form the locus for later Cu–Au mineralization. Potassic alteration overprints both sodic and sodic–calcic alteration assemblages and is best developed in felsic metavolcanic rocks.

Sulfides are associated with stockwork zones of coarse-grained actinolite, magnetite, and apatite, which form steeply dipping breccia bodies. Actinolite in these mineralized zones appears strongly zoned under transmitted light. Sulfide mineralization is associated with a paragenetically late epidote–allanite–calcite–quartz–chlorite–(hematite–thorianite–monazite) assemblage. The interaction of preexisting minerals with the mineralizing fluids resulted in alteration along grain boundaries and fractures. Apatite is overgrown by monazite, allanite, chlorite and quartz/chalcedony. Magnetite displays reaction rims of hematite and quartz, as well as titanite, ilmenite, and rutile veinlets (Fig. 4C). Actinolite is variably altered to chlorite. The resulting mineralized rock displays a breccia texture in which sulfides are concentrated within the matrix around altered clasts containing actinolite, magnetite, apatite, allanite (Fig. 4D), and fragments of actinolitite and massive magnetite bodies. The sulfide assemblage is dominated by chalcopyrite with subsidiary pyrite and Ni-bearing minerals. Siegenite, millerite, and vaesite postdate pyrite and chalcopyrite. Locally, millerite infills fractures in siegenite, but commonly millerite and vaesite show siegenite exsolutions. Pd-melonite, native gold, sphalerite, galena, cassiterite, and hessite represent minor phases and occur as fine-grained inclusions in chalcopyrite.

3.2. Sossego orebody

The Sossego orebody (Fig. 2) occurs northeast of the Sequeirinho orebody and from which it is separated by a major, generally E–W-trending fault. The Sossego orebody is restricted largely to granophyric granite host rocks though some mineralized zones also occur within granite and felsic metavolcanic rocks.

Early sodic alteration at Sossego is poorly developed. It is mainly represented by fracture-controlled albite veinlets that crosscut granite, granophyric granite and felsic metavolcanic rocks outboard of the mineralized zone. Early sodic–calcic alteration and massive magnetite bodies are virtually absent in the Sossego zone.

Pervasive to fracture-controlled vertically focused potassic alteration (biotite–magnetite–quartz and potassium feldspar–calcite–barite–uraninite–galena–sphalerite; Fig. 4E) is the dominant alteration

Table 1
Representative microprobe analyses of amphibole from the Sossego and Sequeirinho orebodies of the Sossego IOCG deposit

	Sequeirinho							Sossego		
	Na–Ca alteration		Na–Ca alteration		Mineralized zone			Mineralized zone		
Sample	252–138	252–138	352–205	352–205	259–211	259–210	259–211	319–112	319–112	319–112
Location	Rim	Core			Rim	Intermediate	Core	Rim	Intermediate	Core
SiO_2	42.47	43.50	53.43	51.90	55.38	54.32	56.29	53.82	54.38	54.31
TiO_2	0.48	0.54	0.11	0.07	0.08	0.16	<0.02	0.08	0.08	0.09
Al_2O_3	8.60	7.74	2.55	2.82	1.47	2.15	0.97	0.92	1.00	0.53
Cr_2O_3	0.06	<0.02	<0.02	<0.02	<0.02	<0.02	0.08	0.02	0.06	<0.02
FeO	22.23	20.96	11.34	16.48	11.02	8.81	10.16	16.51	17.11	17.32
MnO	0.03	0.06	0.08	0.08	0.09	0.03	0.06	0.06	0.04	0.07
MgO	7.68	9.05	16.81	15.15	17.27	18.08	17.54	13.57	13.12	13.02
BaO	<0.02	<0.02	0.25	<0.02	<0.02	0.04	<0.02	0.12	<0.02	<0.02
CaO	11.59	11.62	11.84	11.02	12.56	12.52	12.86	12.07	12.03	12.20
Na_2O	1.50	1.49	0.50	0.22	0.25	0.47	0.20	0.20	0.29	0.15
K_2O	1.29	1.10	0.19	0.13	0.08	0.13	0.05	0.11	0.13	0.09
F	0.30	0.30	0.27	0.04	0.39	0.42	0.16	0.07	0.44	0.69
Cl	3.15	2.86	0.22	0.19	0.11	0.17	0.13	0.12	0.23	0.16
O═Cl·F	0.84	0.77	0.16	0.06	0.19	0.21	0.09	0.06	0.02	0.33
Total	98.52	98.44	97.42	98.03	98.50	97.09	98.40	97.61	98.87	98.30
				Number of ions on the basis of 23 (O,F,Cl)						
TSi	6.647	6.725	7.622	7.358	7.809	7.732	7.937	7.851	7.855	7.893
TAl^{IV}	1.353	1.275	0.378	0.470	0.191	0.268	0.063	0.140	0.145	0.107
TFe^{3}	0.000	0.000	0.000	0.172	0.000	0.000	0.000	0.009	0.000	0.000
CAl^{VI}	0.231	0.133	0.051	0.000	0.053	0.093	0.098	0.000	0.014	0.065
CCr	0.007	0.000	0.001	0.000	0.000	0.000	0.009	0.000	0.002	0.006
CFe^{3}	0.403	0.504	0.513	1.195	0.245	0.170	0.005	0.300	0.261	0.169
CTi	0.057	0.063	0.011	0.007	0.008	0.017	0.001	0.009	0.009	0.009
CMg	1.792	2.086	3.575	3.201	3.629	3.837	3.687	2.574	2.953	2.838
CFe^{2}	2.506	2.205	0.840	0.587	1.054	0.879	1.192	2.110	1.754	1.908
CMn	0.004	0.008	0.009	0.009	0.011	0.004	0.007	0.006	0.008	0.005
BCa	1.943	1.925	1.810	1.674	1.897	1.909	1.942	1.888	1.887	1.871
BNa	0.057	0.075	0.137	0.059	0.069	0.091	0.055	0.031	0.057	0.083
ACa	0.000	0.000	0.000	0.000	0.000	0.000	0.000	0.000	0.000	0.000
ANa	0.398	0.370	0.000	0.000	0.000	0.038	0.000	0.000	0.000	0.000
AK	0.258	0.217	0.035	0.024	0.014	0.023	0.009	0.023	0.020	0.023
Cations	15.02	15.11	14.98	15.94	15.80	15.06	15.01	15.94	14.94	14.98
CCl	0.836	0.748	0.052	0.047	0.027	0.041	0.031	0.058	0.029	0.056
CF	0.148	0.147	0.123	0.017	0.173	0.188	0.070	0.000	0.034	0.200
Mg/(Mg+Fe)	0.42	0.49	0.81	0.85	0.77	0.81	0.76	0.55	0.63	0.60

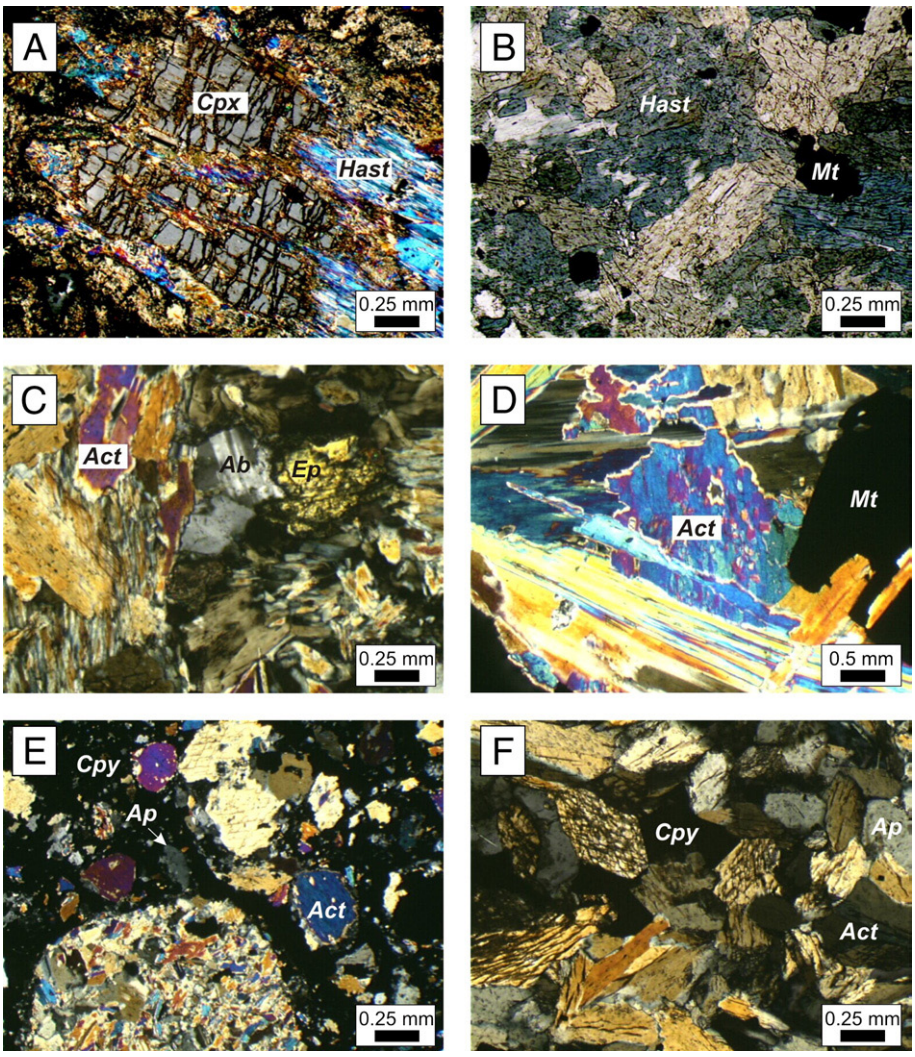

Fig. 5. Photomicrographs showing amphibole generations at the Sossego deposit (transmitted light). A. Fe-edenite/hastingstite in scapolitized gabbro at Sequeirinho. B. Fe-edenite/hastingsite associated with magnetite in hydrothermalized granite close to the gabbro contact (Sequeirinho orebody). C. Actinolite, albite, epidote and titanite assemblage. This association occurs in fracture-controlled and pervasive Na–Ca alteration at Sequeirinho. D. Coarse-grained actinolite in rock composed essentially by amphibole (actinolitite) and magnetite (crossed polars). E. Actinolite crystals and actinolitite fragments within a chalcopyrite matrix in the Sequeirinho breccia (crossed polars). F. Euhedral actinolite crystals associated with apatite, quartz, and chalcopyrite in the matrix of the Sossego breccia (crossed polars). Abbreviations: Ab = albite; Act = actinolite; Ap = apatite; Cc = calcite; Cpx = clinopyroxene; Cpy = chalcopyrite; Ep = epidote; Hast = hastingsite/ferro-edenite; Mt = magnetite.

type preserved in the Sossego orebody (Fig. 3). It occurs in replacement zones close to mineralized zones, which commonly show intense red color due to tiny inclusions (<5 μm) of hematite within the potassium feldspar. Within these zones, potassium feldspar mantles on albite rims or occurs as fracture infill in albite. Zones of most intense potassic alteration are dominated by pervasive rock replacement by biotite with associated potassium feldspar and magnetite that grade outward to chlorite enriched zones. Potassically altered rocks at Sossego are intensely affected by later chloritization and calcite veining with subordinate quartz, titanite, rutile, pyrophanite, and magnetite.

Mineralization at Sossego occurs within vein networks, crackle breccia zones, and breccia pipes that cut potassically altered and chloritized rocks. The breccias contain angular to rounded clasts of granitic wallrocks rimmed by magnetite. The matrix is dominated by hydrothermal minerals with open-space filling textures. Infill in veins and breccias at Sossego consists of magnetite–actinolite–apatite–biotite–calcite–epidote with minor sulfides cut by sulfides, Fe-chlorite, quartz, calcite, epidote, and muscovite–(sericite). Sulfides are dominated by chalcopyrite and pyrite with lesser siegenite, millerite, vaesite, native gold, hessite, Pd-melonite, cassiterite (Fig. 4F), and molybdenite.

The latest stage of alteration at Sossego is represented by an assemblage of muscovite–hematite–quartz–chlorite–calcite that

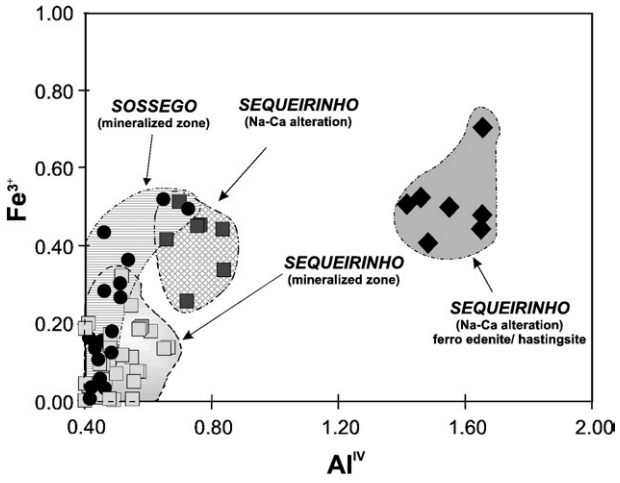

Fig. 6. Al^{IV} (pfu) *vs.* Fe^{3+} (pfu) diagram for the Sossego and Sequeirinho amphiboles.

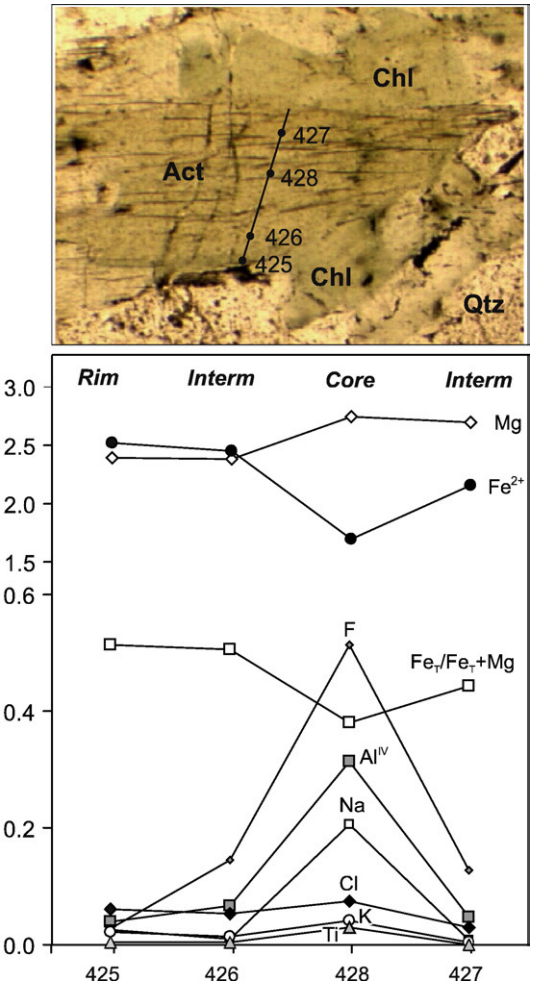

Fig. 7. Compositional variations in fragment of zoned amphibole within a chlorite–quartz matrix from mineralized breccia of the Sossego orebody.

occurs locally in intensely fractured zones cutting mineralized breccias. Such zones are generally poorly mineralized and appear to represent a late, high-level zone of hydrolytic alteration.

4. Analytical methods

Documentation of the paragenetic sequence of hydrothermal alteration and mineralization in the Sossego deposit was carried out based on mapping at the mine site and the surrounding areas, detailed drill core descriptions, petrographic studies under transmitted and reflected light, cathodoluminescence studies, and scanning electronic microscopy.

Mineral analyses were obtained by a CAMECA CAMEBAX SX50 electron microprobe at the Microprobe Laboratory, Instituto de Geociências, Universidade de Brasília. The wavelength dispersive technique was employed, with accelerating voltages of 15 kV and probe current of 25 μA for all elements, except As, Ag, Sb, Au, Co, Se, Zn, Ni, Cu, Fe, Pd, Te, Th, and S, which were analyzed using accelerating voltages of 20 kV and probe current of 40 μA. On-peak count times of 10 s and beam diameters of 10 μm and 5 μm were used for halogens and other elements, respectively.

A variety of well-characterized standards were used to calibrate all elements, including: natural Mn-hortonolite (olivine) for Si, Fe, Mn, and Mg, barium feldspar ($BaAlSi_2O_8$) for Ba, microcline for K and apatite for P, and synthetic anorthite-100 (plagioclase glass) for Al and Ca, anorthite-50 (plagioclase glass) for Na, chromite for Cr, rutile for Ti,

Table 2
Representative microprobe analyses of feldspar from the Sequeirinho orebody

Mineral	Albite	Albite	Albite	Albite	K feldspar	K feldspar
Sample	352–138	352–138	352–205	352–205	352–138	352–138
SiO_2	67.77	67.52	67.92	68.01	64.95	64.57
TiO_2	0.02	<0.02	0.03	<0.02	<0.02	<0.02
Al_2O_3	19.85	19.83	19.61	19.63	18.48	18.39
Cr_2O_3	<0.02	<0.02	<0.02	0.04	0.03	0.03
FeO	0.10	0.06	0.19	<0.02	0.07	<0.02
MnO	0.02	<0.02	0.02	<0.02	<0.02	<0.02
MgO	<0.02	0.02	0.02	<0.02	<0.02	<0.02
BaO	0.13	0.07	0.03	<0.02	0.04	0.15
ZnO	<0.02	<0.02	0.08	<0.02	0.03	0.02
CaO	0.72	0.72	0.20	0.22	<0.02	<0.02
Na_2O	11.44	11.55	11.94	11.78	0.20	0.23
K_2O	0.08	0.10	0.10	0.08	17.01	16.72
Total	100.13	99.87	100.14	99.76	100.81	100.11
	Number of ions on the basis of 16 O					
Si	5.948	5.944	5.971	5.970	5.993	5.990
Al	2.052	2.056	2.030	2.030	2.007	2.009
Cr	0.000	0.000	0.000	0.000	0.000	0.000
Ti	0.001	0.000	0.002	0.000	0.000	0.000
Fe^{2+}	0.007	0.004	0.014	0.001	0.005	0.001
Mn	0.001	0.000	0.001	0.001	0.000	0.000
Mg	0.000	0.003	0.002	0.000	0.000	0.000
Ba	0.005	0.002	0.001	0.000	0.001	0.005
Zn	0.000	0.000	0.010	0.000	0.000	0.000
Ca	0.068	0.068	0.019	0.021	0.000	0.000
Na	1.947	1.971	2.035	2.006	0.036	0.042
K	0.009	0.012	0.011	0.009	2.002	1.979
Ab	96.200	96.100	98.500	98.500	1.800	2.100
An	3.400	3.300	0.900	1.000	0.000	0.000
Or	0.400	0.600	0.500	0.400	98.200	97.900

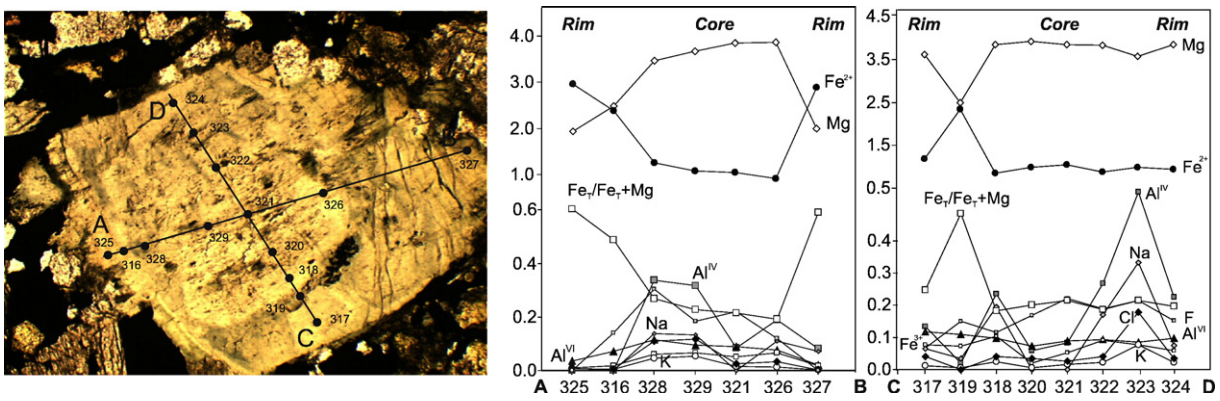

Fig. 8. Compositional variations in zoned amphibole from mineralized breccia of the Sequeirinho orebody.

thorite for Th, vanadium trioxide for V, and zincite for Zn in silicates. For analyses of sulfide minerals natural standards for Fe and S (pyrite), Cu (chalcopyrite) and Pb (galena) and synthetic standards for Zn (sphalerite), As (iron arsenide, $FeAs_2$), Se (zinc selenide, ZnSe) and Ag, Sb, Au, Co, Ni, Pd, and Te (metal) were used. Fluorine and chlorine were calibrated using synthetic fluorite and chloro-apatite, respectively, and analyzed using TAP 1 and PET 2 spectrometer crystals. Routine minimum limits of detection were 0.05 elemental wt.% for F and 0.02 elemental wt.% for all other elements.

The raw electron-microprobe data were reduced using Probe software, which uses standard ZAF correction algorithms. The data were analyzed using spreadsheet routines, Minpet 2.02 (Richard, 1997), Gpt (Reche and Martinez, 1996), Twq 2.02 (Berman, 1988, 1991), Twq File Archivist 1.0 (Juliani, 2000), and HbPl 1.2 software (Holland and Blundy, 1995).

5. Mineral chemistry

5.1. Amphibole

Representative compositions of amphibole from sodic–calcic alteration and mineralization zones of the Sossego and Sequeirinho orebodies are shown in Table 1. Cationic compositions were recalculated on the 23 (O, F, Cl) basis, assuming a total of 13 cations except Ca, Na, and K (13 CNK).

5.1.1. Sodic–calcic alteration

Two different amphibole types occur in sodic–calcic alteration zones from the Sequeirinho orebody (Fig. 5A–D). The first occurs mainly in restricted haloes close to granite and gabbro contacts replacing both rocks (Fig. 5A, B). It has a ferro-edenite to hastingsite

Table 3
Representative microprobe analyses of biotite from the Sossego orebody of the Sossego IOCG deposit

Sample	314–195	314–195	314–195	314–195	314–195	314–195
Analysis	359	360	361	362	364	365
SiO_2	36.05	36.61	36.49	36.71	36.07	36.34
TiO_2	2.29	2.18	2.14	1.95	1.83	2.25
Al_2O_3	11.45	11.21	11.41	11.97	11.70	11.44
Cr_2O_3	<0.02	<0.02	0.02	0.02	0.04	<0.02
Fe_2O_3	5.12	5.14	5.34	5.90	5.35	4.96
FeO	22.29	22.40	21.81	22.34	21.82	22.79
MnO	0.09	0.05	0.05	0.06	0.04	0.05
MgO	7.87	7.36	8.47	8.57	8.77	7.63
BaO	<0.02	<0.02	<0.02	<0.02	0.17	0.09
CaO	0.06	0.02	0.07	0.01	<0.02	0.04
Na_2O	0.12	0.04	0.07	0.03	0.02	<0.02
K_2O	9.10	9.23	8.81	7.86	8.71	9.27
CuO	0.12	<0.02	0.05	<0.02	<0.02	<0.02
F	0.20	0.24	0.14	0.07	<0.05	0.23
Cl	2.61	2.74	2.26	2.57	2.49	3.06
O_F_Cl	0.67	0.72	0.57	0.61	0.56	0.79
Total	96.79	95.49	95.67	95.27	96.50	97.40
Number of ions on the basis of 24 (O, F, Cl, OH)						
Si	5.742	5.604	5.558	5.388	5.698	5.855
$Al^{(IV)}$	2.169	2.079	2.105	2.202	2.179	2.145
$Al^{(VI)}$	0.000	0.000	0.000	0.000	0.000	0.027
Ti	0.277	0.258	0.252	0.229	0.217	0.273
Fe^{3+}	0.619	0.609	0.629	0.693	0.636	0.602
Fe^{2+}	2.996	2.949	2.857	2.918	2.882	3.071
Cr	0.001	0.000	0.003	0.003	0.005	0.000
Mn	0.012	0.007	0.007	0.008	0.005	0.007
Mg	1.886	1.726	1.977	1.994	2.065	1.833
Ba	0.000	0.000	0.000	0.000	0.011	0.006
Ca	0.010	0.003	0.012	0.002	0.000	0.006
Na	0.036	0.012	0.022	0.010	0.005	0.001
K	1.866	1.853	1.760	1.565	1.755	1.906
Cu	0.015	0.000	0.006	0.000	0.000	0.000
Cations	15.63	15.10	15.19	15.01	15.46	15.73
CF	0.204	0.235	0.135	0.066	0.019	0.236
CCL	1.421	1.461	1.201	1.360	1.330	1.673
OH	2.804	3.977	4.033	4.324	3.156	1.971
Mg/(Mg+Fe)	0.39	0.37	0.41	0.41	0.42	0.37
XF	0.05	0.04	0.03	0.01	0.00	0.06
XCl	0.32	0.26	0.22	0.24	0.30	0.43
XOH	0.63	0.70	0.75	0.75	0.70	0.51
X_{sid}	0.12	0.11	0.12	0.19	0.13	0.11
X_{ann}	0.49	0.52	0.47	0.41	0.45	0.52
IV(F)	1.96	2.03	2.32	2.64	3.07	1.73
IV(Cl)	−5.46	−5.29	−5.27	−5.29	−5.44	−5.66
IV(F/Cl)	7.41	7.31	7.59	7.93	8.51	7.38
Calculation temperature=500 °C						
log (fH_2O)/(fHF)	5.18	5.25	5.55	5.89	6.31	4.95
log (fH_2O)/($fHCl$)	2.74	2.87	2.98	2.96	2.84	2.50
log (fHF)/($fHCl$)	−3.00	−2.91	−3.15	−3.51	−4.06	−2.98
Calculation temperature=400 °C						
log (fH_2O)/(fHF)	5.72	5.78	6.10	6.43	6.85	5.48
log (fH_2O)/($fHCl$)	3.00	3.13	3.25	3.22	3.11	2.77
log (fHF)/($fHCl$)	−3.35	−3.26	−3.52	−3.87	−4.43	−3.33

log (fHF)/($fHCl$), log (fH_2O)/($fHCl$) and log (fH_2O)/(fHF) of the fluid in equilibrium with the Sossego biotite were calculated according to Zhu and Sverjenski (1992).

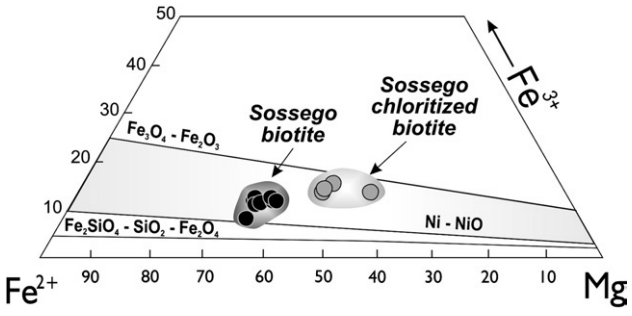

Fig. 9. Composition of biotite from potassic alteration zones of the Sossego orebody in terms of Fe^{3+}–Fe^{2+}–Mg (Wones and Eugster, 1965). FeO and Fe_2O_3 were estimated according to De Bruyin et al. (1983). Cationic proportions based on 24 (O, OH, F, Cl).

composition with $(Na+K)_A$ values higher than 0.50, average # Mg values of 0.42, and high chlorine contents (up to 3.77 wt.% or 1.02 atoms pfu). This amphibole is zoned with cores characterized by high Fe^{3+} contents (Fig. 6), whereas rims are enriched in Fe^{2+}, Al^{IV}, Al^{VI}, $(Na+K)_A$, and Cl. The second amphibole occurs in fracture-controlled pervasive sodic–calcic alteration zones (Fig. 5C, D) and commonly replaces the ferro-edenite/hastingsite. Its composition is close to the boundary between actinolite and magnesiohornblende, with $(Na+K)_A$ less than 0.50, and average # Mg values of 0.78. Chlorine contents (up to 0.68 pfu) in actinolite and magnesiohornblende are significantly lower than those of ferro-edenite/hastingsite.

5.1.2. Mineralized zones

Amphibole is an important hydrothermal mineral phase in the mineralized breccias from the Sequeirinho and Sossego orebodies (Fig. 5E, F). At Sossego, the amphibole is actinolite to subordinate ferro-actinolite (Leake et al., 1997) with average # Mg value of 0.58. At Sequeirinho, amphibole from mineralized breccias is actinolite to ferro-actinolite with average # Mg values of 0.74, similar to that of amphibole from the sodic–calcic alteration zones from this orebody. In both orebodies, the coarse-grained (up to 5 cm) amphibole crystals from mineralized zones are strongly zoned under transmitted light. In the Sossego orebody, a general trend of increase of Fe^{2+} contents and Fe/(Fe+Mg) ratios accompanied by decrease of Al^{IV}, Al^{VI}, Ti, Na, and K towards crystal rims is identified (Fig. 7). Amphibole from mineralized breccia at

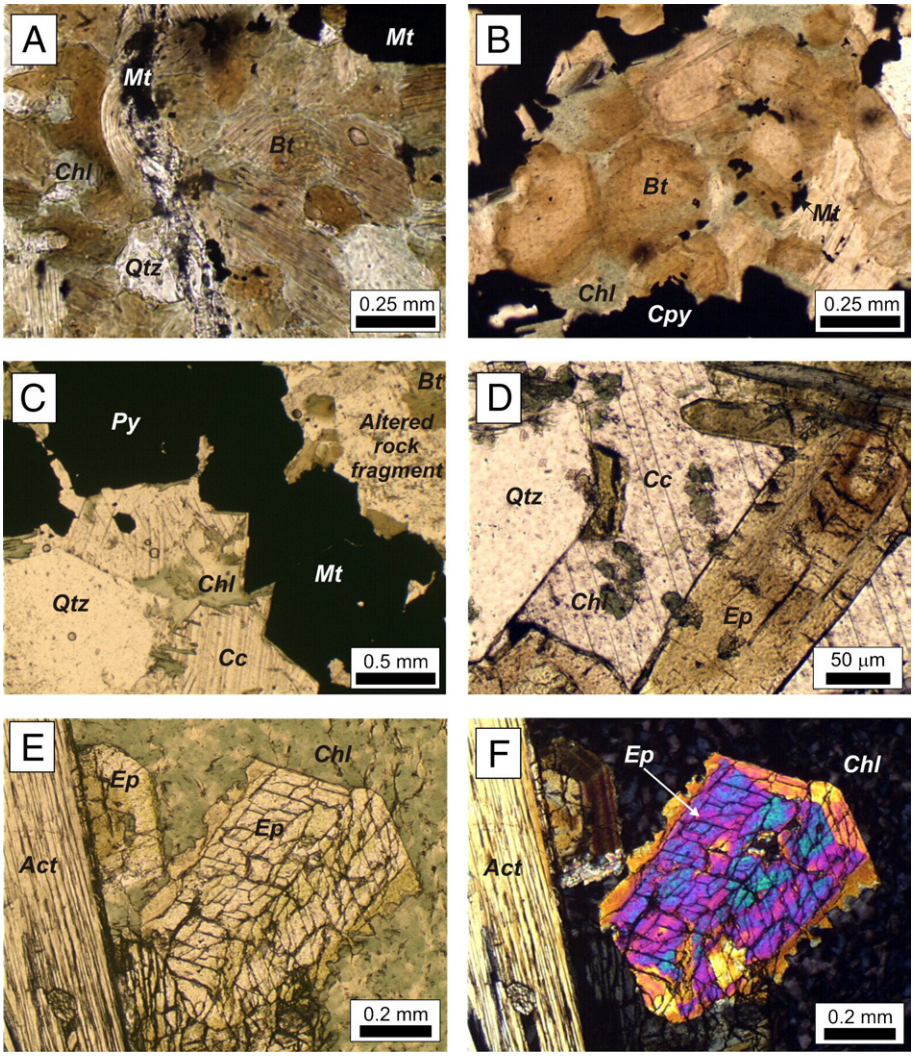

Fig. 10. A and B. Biotite–magnetite–quartz assemblage associated with potassic alteration at Sossego (transmitted light). C. Sossego mineralized breccia with fragments of granophyric granite replaced by biotite and potassium feldspar and rimmed by magnetite–(pyrite). Calcite, quartz, chlorite predominate within the breccia matrix (transmitted light). D. Zoned epidote crystals with REE-enriched cores associated with calcite, quartz, and chlorite in breccia matrix at Sossego (transmitted light). E. Zoned epidote associated with actinolite and late chlorite (Sossego ore breccia; transmitted light). F. As E with crossed polars. Abbreviations: Bt = biotite; Cc = calcite; Chl = chlorite; Cpy = chalcopyrite; Ep = epidote; Hast = hastingsite/ferro-edenite; Mt = magnetite; Qtz = quartz; Py = pyrite.

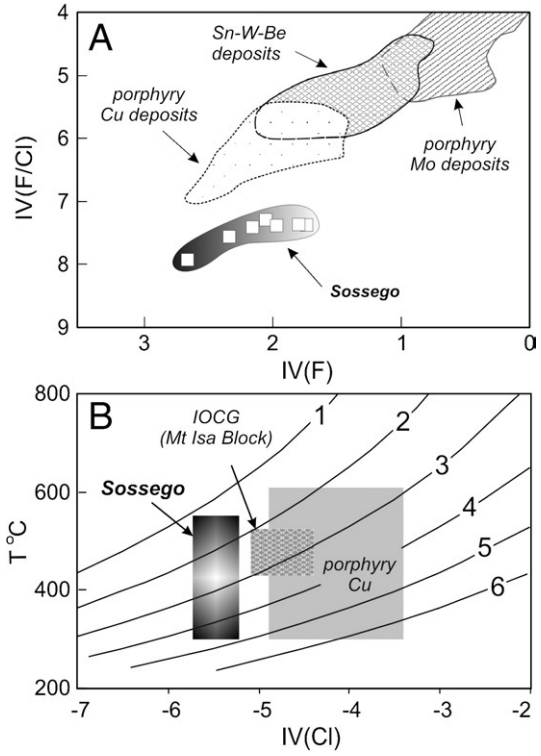

Fig. 11. A. Fluorine intercept [IV(F)] *vs.* fluorine/chlorine intercept [IV(F/Cl)] diagram for the Sossego biotite and fields for magmatic-hydrothermal (Munoz, 1984); B. relation between chlorine intercept [IV(Cl)], temperature and fluid composition for biotite from Sossego, porphyry copper deposits (Munoz, 1984), and IOCG deposits from the Mt Isa Block. [IV(Cl)] values for biotite from the Mt Isa Block were calculated based on X_{Mg} and log (XCl/XOH) values of Marshall and Oliver (2006). Diagonal lines represent contours of log (fH_2O)/(fHCl) calculated for wide temperature range and chlorine intercept values using equations of Munoz (1984, 1992).

Sequeirinho exhibits more complex zoning patterns. Commonly, amphiboles have darker rims, which show higher Fe^{2+} contents and Fe/(Fe+Mg) than crystal cores. Some crystals, however, are characterized by increased Fe^{2+} towards borders and overgrowth of a paler rim with lower Fe^{2+} contents (Fig. 8). Higher Al^{IV}, Al^{VI}, Na, K, and Cl contents are observed in intermediate parts of the crystals. The $Al^{(IV)}$ and Fe^{3+} contents of amphibole from mineralized zones of the Sossego and Sequeirinho orebodies (Fig. 6) are similar to those known from >2 kbar settings elsewhere (e.g., Cloncurry; De Jong and Williams, 1995).

5.2. Feldspar

Representative compositions of feldspar from the Sequeirinho orebody are shown in Table 2. Felspar from sodic–calcic alteration zones has albite composition. In restricted haloes close to the contact between gabbro and granite, albite occurs associated with ferro-edenite or hastingsite and has $An_{0.4–3.4}$ and $Ab_{96–99}$. In pervasive sodic–calcic alteration zones, chessboard albite occurs associated with actinolite and magnesiohornblende and has a narrow compositional variation ($An_{0.8–1.2}$ and $Ab_{98–99}$). In the Sequeirinho orebody, orthoclase (Or_{98}–$An_{0.0–0.5}$–$Ab_{1.9–2.1}$) occurs in poorly developed potassic alteration zones.

5.3. Biotite

Representative compositions of biotite from the potassic alteration zones of the Sossego orebody are shown in Table 3. Structural formulae were recalculated on the basis of 24 (O, OH, F, Cl). FeO and Fe_2O_3 contents were estimated according to methods of De Bruyin et al. (1983). The Sossego hydrothermal biotite has intermediary composition between annite and phlogopite with X_{ann} values between 0.32 and 0.52. Fe^{2+}–Fe^{3+}–Mg compositions indicate fO_2 conditions above the Ni–NiO buffer for the biotite crystallization (Fig. 9). These conditions are compatible with the association between biotite and magnetite observed in potassic alteration zones and with absence of hematite (Fig. 10A, B).

Biotite is also characterized by high chlorine (up to 3.06 wt.% or 1.72 pfu), which corresponds to up to 58 mol% of the OH site occupancy. The variation of Mg/(Fe+Mg) is actually quite small, and it is not clear if chlorine incorporation in biotite is controlled by Mg–Cl avoidance mechanisms.

5.3.1. Halogen activities in the hydrothermal fluid

Halogens substitution in biotite and amphibole is a function of temperature of hydroxyl-halogen exchange, pressure, fluid composition represented by activity of halogen ion or halogen acid present during crystallization, and crystal chemistry (Munoz, 1984, 1992; Zhu and Sverjensky, 1992; Zhu et al., 1994). Additionally, post-crystallization leaching or enrichment due to later interaction with hydrothermal fluids should be also considered.

Due to crystal chemistry control on halogen incorporation, the content of halogens in biotite by themselves might be an inadequate measure of relative halogen enrichment. Thus, fluorine [IV(F)], chlorine [IV(Cl)], and fluorine/chlorine [IV(F/Cl)] intercept values were introduced to define single numerical values to measure relative enrichment corrected for effects of Fe–F and/or Mg/Cl avoidance (Munoz, 1984), permitting comparisons with biotite with different Mg/Fe ratios.

The calculated fluorine intercept values [IV(F)] for Sossego biotite vary from 1.7 to 2.6. These values are higher than those values typical of F-enriched micas and overlap the range for biotite from common igneous rocks, barren systems, and porphyry-Cu deposits (Munoz, 1984; Fig. 11A).

Fluorine/chlorine intercept values [IV(F/Cl)=7.3 to 7.9] are significantly higher than those estimated for porphyry-Cu deposits (Fig. 11A). Because the [IV(F/Cl)] values are directly related to the fugacity ratio f(HCl)/f(HF) of the fluid at constant temperature (Munoz, 1984, 1992), these higher values may correspond to higher Cl/F ratios in the fluid. However, the effect of temperature uncertainty should be evaluated in the Sossego deposit. Fig. 11B shows biotite composition in terms of [IV(Cl)] against a wide temperature range (550 to 300 °C) and contours of fluid composition in terms of log [(fH_2O)/(fHCl)]. Similar fluid composition could result in distinct biotite composition in porphyry-Cu and IOCG deposits, including Sossego and deposits from the Mt Isa Block, Australia (Marshall and Oliver, 2006), if differences in final exchange temperatures are considered.

5.4. Chlorite

Representative compositions of chlorite from the mineralized zones of the Sossego (Fig. 10C) and Sequeirinho orebodies are shown in Table 4. According to AIPEA Nomenclature Committee recommendations for nomenclature of the trioctahedral chlorite (Bailey, 1980), chlorite from the two orebodies has composition between the clinoclore [$(Mg_5Al)(Si_3Al)O_{10}(OH)_8$] and chamosite [$(Fe^{2+}_5Al)(Si_3Al)O_{10}(OH)_8$] end-members.

Sequeirinho chlorite has $Fe^{2+}/(Fe^{2+}+Mg)$ ratios between 0.50 and 0.60. Sossego chlorite has $Fe^{2+}/(Fe^{2+}+Mg)$ slightly lower (0.48 to 0.56) than chlorite from Sequeirinho and biotite from Sossego. The latter indicates that the chlorite composition is not controlled only by inheritance of the parent mineral chemistry, but could reflect change in the physical–chemical conditions with increase of fO_2 and fS_2 conditions related to oxidation and sulfidization processes (Bryndzia and Scott, 1987).

Table 4
Representative microprobe analyses of chlorite from the Sequeirinho and Sossego orebodies of the Sossego IOCG deposit

Sample	Sequeirinho				Sossego			
	259–211	259–211	259–211	352–138	314–195	314–195	314–195	314–195
Analysis	477	465	466	468	368	374	377	393
SiO_2	25.82	25.90	26.98	27.52	27.65	25.19	24.57	25.37
TiO_2	0.02	0.02	0.02	0.14	0.06	0.03	<0.02	0.10
Al_2O_3	19.91	18.85	18.49	15.96	17.26	20.40	21.12	20.65
Cr_2O_3	<0.02	<0.02	<0.02	0.04	<0.02	0.01	0.04	<0.02
Fe_2O_3	0.23	0.44	0.64	0.56	0.55	1.01	0.22	0.72
FeO	26.19	30.01	26.06	30.25	25.70	26.72	27.99	26.54
MnO	0.06	0.10	0.11	0.14	0.12	0.07	0.07	0.07
MgO	14.91	12.25	15.10	12.62	15.68	13.43	12.61	13.70
BaO	<0.02	<0.02	0.08	<0.02	0.12	0.03	<0.02	0.12
ZnO	<0.02	<0.02	0.09	0.04	0.01	<0.02	<0.02	<0.02
CaO	0.02	0.14	0.06	0.17	0.04	0.03	0.01	0.04
Na_2O	<0.02	<0.02	<0.02	<0.02	0.04	<0.02	<0.02	<0.02
K_2O	0.02	<0.02	0.02	0.06	0.03	0.07	0.10	0.01
F	0.07	0.17	0.17	<0.02	0.14	0.51	<0.02	0.20
Cl	0.05	0.01	0.08	0.19	0.02	0.13	0.11	0.08
H_2O	11.15	10.90	11.08	10.91	11.12	10.58	11.00	10.97
Total	98.43	98.79	98.97	98.59	98.52	98.21	97.86	98.57
O_F_Cl	0.04	0.07	0.09	0.04	0.06	0.24	0.02	0.10
Total	98.39	98.72	98.88	98.54	98.46	97.97	97.84	98.46
	Number of ions on the basis of 36 (O, OH, F, Cl)							
Si	5.492	5.587	5.695	5.974	5.86	5.343	5.317	5.391
Al^{IV}	2.508	2.413	2.305	2.026	2.14	2.657	2.683	2.609
Al^{VI}	2.492	2.397	2.317	2.070	2.19	2.495	2.714	2.590
Ti	0.003	0.003	0.002	0.022	0.01	0.004	0.002	0.015
Cr	0.000	0.000	0.000	0.006	0.00	0.001	0.007	0.000
Fe^{3+}	0.036	0.072	0.102	0.092	0.09	0.161	0.036	0.115
Fe^{2+}	4.658	5.414	4.601	5.493	4.55	4.740	5.066	4.717
Mn	0.011	0.018	0.020	0.026	0.02	0.013	0.013	0.013
Mg	4.726	3.940	4.751	4.085	4.95	4.247	4.066	4.340
Zn	0.000	0.000	0.014	0.007	0.00	0.000	0.000	0.000
Ca	0.004	0.032	0.013	0.040	0.01	0.007	0.003	0.009
Na	0.000	0.000	0.000	0.000	0.03	0.000	0.000	0.000
K	0.009	0.000	0.009	0.035	0.02	0.038	0.056	0.004
Ba	0.000	0.000	0.013	0.000	0.02	0.004	0.000	0.020
CF	0.093	0.228	0.228	0.000	0.18	0.679	0.000	0.272
CC	0.037	0.006	0.054	0.136	0.01	0.090	0.078	0.060
OH	15.870	15.766	15.718	15.864	15.81	15.231	15.922	15.669
Total	35.940	35.876	35.842	35.876	35.89	35.710	35.964	35.823
Fe/(Fe+Mg)	0.50	0.58	0.50	0.58	0.48	0.54	0.56	0.53

Fe^{2+}, Fe^{3+} and OH were calculated assuming full site occupancy.

Chlorine contents in the Sossego chlorite (up to 0.12 wt.%) are lower than those of the Sossego biotite, but fluorine contents (0.50 wt.%) are elevated (Fig. 12). This could reflect preferential fluorine incorporation in the OH site due to higher Mg/(Mg+Fe) ratios of chlorite or residual fluorine concentration in the late fluids responsible by the chloritization. The Sequeirinho chlorite has fluorine and chlorite contents of up to 0.17 and 0.32 wt.%, respectively.

$Al^{(IV)}$ contents in the Sossego chlorite display strong positive correlation with Fe/(Fe+Mg) ratios, which is expressed by the equation: $Al^{(IV)} = 0.90 * Fe/(Fe+Mg) + 1.67$ (Fig. 12). This indicates that replacement of Si by $Al^{(IV)}$ was accompanied by substitution of Mg by Fe. Similar correlation between $Al^{(IV)}$ contents and Fe/(Fe+Mg) ratios was not observed in chlorite from the Sequeirinho orebody.

5.5. Magnetite

Magnetite from the Sequeirinho orebody has low TiO_2 contents (0.01 to 0.11 wt.%) and relatively high V_2O_3 (0.42 to 0.66 wt.%), ThO_2 (up to 850 ppm), PbO (up to 720 ppm), and P_2O_5 (530 ppm) contents (Table 5). Sossego magnetite has higher TiO_2 (0.04 to 0.87 wt.%) and lower V_2O_3 (0.05 to 0.29 wt.%) contents than Sequeirinho magnetite. It is also richer in Al, Si (Fig. 13A), Ca, Pb, Th, and Zn compared to magnetite from Sequeirinho.

The highest TiO_2 in Sossego magnetite could reflect submicroscopic exsolution of ilmenite or rutile, which were identified in SEM studies (Fig. 13). However, the overall Ti content (pfu) and Ti/V ratios (Fig. 13B) of magnetite from Sossego are similar to those reported for IOCG deposits elsewhere (Beaudoin et al., 2006; Gosselin et al., 2006).

The compositions of Sequeirinho magnetite, which are closely related to sodic–calcic alteration, however, overlap those from magnetite–apatite deposits of Kiruna type in terms of Ti, Ti/V, Si and Al (Beaudoin et al., 2006).

5.6. Sulfides

5.6.1. Chalcopyrite and pyrite

Chalcopyrite from the Sossego and Sequeirinho orebodies (Fig. 14A, B) has composition close to the ideal chalcopyrite ($CuFeS_2$). Some crystals, however, display high Se (up to 2500 ppm at Sossego and 1870 ppm at Sequeirinho) contents.

Pyrite has high Co (up to 2.27% in Sossego and 1.97% in Sequeirinho), Ni (up to 1810 ppm and 1790 ppm, respectively), and Se (5000 ppm and 4530 ppm; Table 6) contents. Negative correlation between Se and S and Fe and Co–Ni implies incorporation of these elements in the sulfide structure. Co/Ni ratios in pyrite from Sossego (6 to 163) and Sequeirinho (10 to 158) display a wide variation. The lowest Co/Ni ratios are close to those from magmatic systems (Fig. 15). However, the majority of the samples have higher Co/Ni ratios than those typical of magmatic, volcanogenic and sedimentary sulfides.

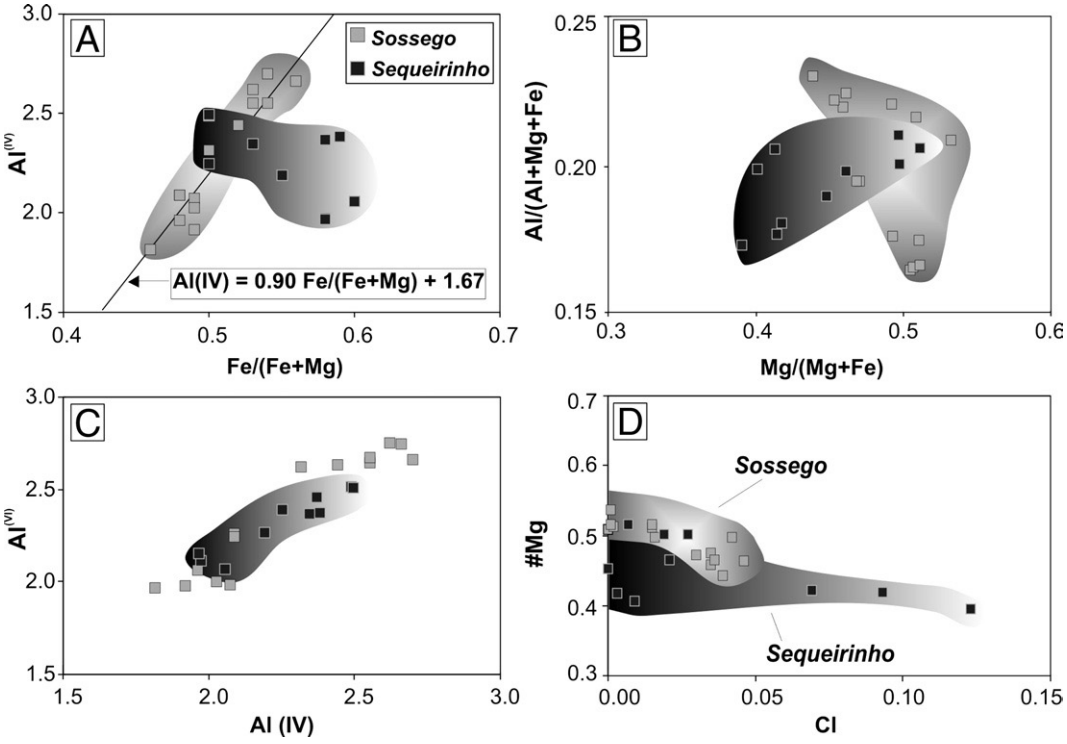

Fig. 12. A. Fe/(Fe+Mg) *vs.* Al^{IV}; B. Mg/(Fe+Mg) *vs.* Al/(Al+Fe+Mg); C. Al^{IV} *vs.* Al^{VI}; and D. Cl (pfu) *vs.* Mg/(Fe+Mg) binary plots for chlorite from mineralized zones from the Sossego and Sequeirinho orebodies.

5.6.2. Siegenite, millerite and native gold

Siegenite [ideal formulae: $(Ni,Co)_3S_4$] is an important accessory mineral phase in the Sossego and Sequeirinho orebodies (Fig. 14C) and commonly occurs associated with chalcopyrite. It has an intermediate composition between the end-members polydymite ($NiNi_2S_4$) and linnaeite ($CoCo_2S_4$), and significant Cu and Fe contents are present. Sossego and Sequeirinho siegenite has Fe contents between 0.5 and 9.0 wt.%. Contents of Cu from 0.2 to 1.1 wt.% and high Se (up to 5600 ppm) are also verified (Table 6).

Millerite (NiS) occurs as inclusion in chalcopyrite (Fig. 14B) in association with siegenite and pyrite in the Sossego and Sequeirinho orebodies. Fe contents in millerite range from 0.4 to 1.1 wt.%. High Co (up to 5130 ppm), Cu (up to 1580 ppm), and Pd (up to 1130 ppm) are also observed (Table 6).

In the Carajás Mineral Province, siegenite was previously recognized in the Igarapé Bahia IOCG deposit (Tallarico et al., 2005), where it occurs associated with uraninite, monazite, and cobaltite. Millerite was also reported for the Cristalino IOCG deposit in the Carajás Mineral Province (Huhn et al., 2000). In this deposit, millerite occurs associated with chalcopyrite, pyrite, magnetite, bravoite, cobaltite, vaesite, and native gold.

Native gold occurs either as sub-μm-sized inclusions or coarse-grained slabs of up to 100 μm in chalcopyrite (Fig. 14D). Microprobe analyses indicate Ag contents between 10.7 and 14.9 wt.% in native gold from the Sossego and Sequeirinho orebodies.

Table 5
Representative microprobe analyses of magnetite from the Sossego orebody of the Sossego IOCG deposit

Sample	Sequeirinho			Sossego			
	259_210	259_210	259_210	314_195	314_195	314_195	319_112
SiO_2	0.03	0.02	<0.02	0.36	0.10	1.76	0.38
TiO_2	<0.02	0.10	0.11	0.04	0.24	0.16	0.63
Al_2O_3	0.09	0.07	0.11	0.08	0.03	0.34	0.17
Cr_2O_3	0.02	<0.02	<0.02	<0.02	<0.02	<0.02	0.03
V_2O_3	0.66	0.46	0.42	0.13	0.27	0.13	0.17
Fe_2O_3	68.77	68.74	68.39	68.46	68.07	66.86	67.22
FeO	31.03	31.15	31.03	30.81	31.04	30.26	31.19
MnO	<0.02	0.02	<0.02	<0.02	<0.02	0.02	<0.02
MgO	<0.02	<0.02	<0.02	0.07	0.02	0.19	0.17
ZnO	<0.02	<0.02	<0.02	<0.02	<0.02	<0.02	<0.02
CaO	<0.02	<0.02	<0.02	0.05	0.02	0.33	0.06
ThO_2	<0.02	0.09	0.05	<0.02	0.11	<0.02	0.07
PbO	<0.02	<0.02	0.07	<0.02	0.06	0.04	<0.02
Total	100.61	100.65	100.19	100.00	99.94	100.08	100.10
Number of ions on the basis of 32 (O)							
Si	0.009	0.006	0.000	0.109	0.031	0.533	0.118
Al	0.031	0.024	0.038	0.030	0.010	0.119	0.060
Cr	0.005	0.002	0.000	0.000	0.000	0.000	0.006
V	0.132	0.092	0.086	0.025	0.055	0.025	0.033
Fe^{3+}	15.782	15.798	15.796	15.790	15.769	15.188	15.470
Ti	0.003	0.024	0.026	0.009	0.055	0.037	0.144
Mg	0.000	0.000	0.004	0.032	0.009	0.085	0.079
Fe^{2+}	7.915	7.956	7.964	7.897	7.990	7.639	7.978
Zn	0.000	0.000	0.000	0.000	0.000	0.000	0.002
Mn	0.000	0.004	0.000	0.000	0.000	0.004	0.000
Pb	0.000	0.000	0.006	0.000	0.005	0.003	0.000
Th	0.000	0.006	0.003	0.001	0.007	0.000	0.005
Ca	0.003	0.004	0.000	0.015	0.005	0.105	0.020
Total	23.880	23.916	23.924	23.917	23.936	23.738	23.915

6. Geothermobarometry and stability fields of the hydrothermal associations

6.1. Sodic–calcic alteration

Sodic–calcic alteration represents the main alteration type in the Sequeirinho orebody. Temperature conditions for this alteration stage were estimated based on the plagioclase–amphibole geothermometer of Holland and Blundy (1994). This geothermometer was calibrated for amphibole (Na_A>0.02 pfu, $Al^{(VI)}$<1.8 pfu, and Si between 6.0 and 7.7 pfu) and plagioclase (X_{an}<0.90) assemblages in the temperature range of 400 to 900 °C. Actinolite/magnesiohornblende and albite from pervasive sodic–calcic alteration zones display compositional variation within the calibration range defined by Holland and Blundy

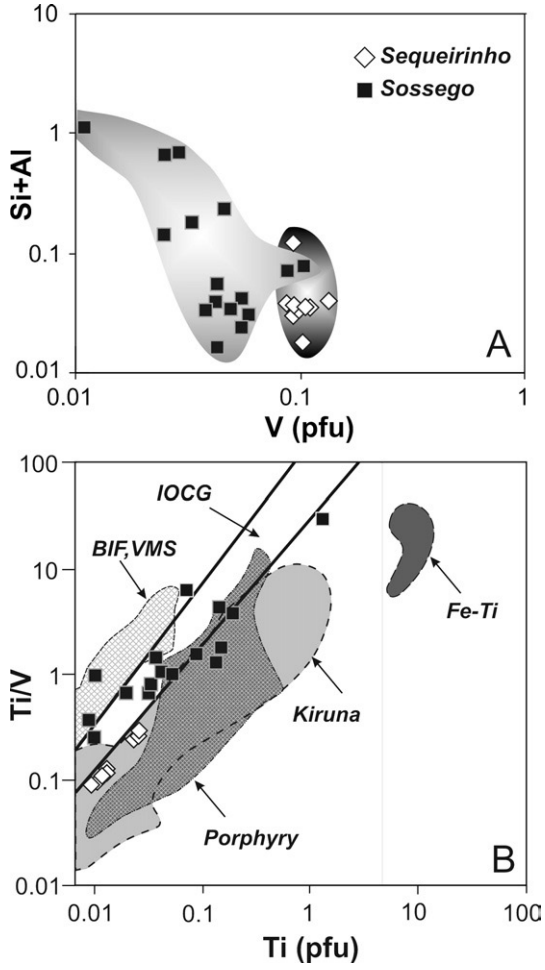

Fig. 13. Vanadium (pfu) *vs.* Si+Al (A) and Ti (pfu) *vs.* Ti/V (B) binary plots for magnetite from the Sossego and Sequeirinho orebodies. Fields for magnetite from IOCG, Kiruna, porphyry, VMS, BIF, and Fe–Ti deposits based on Beaudoin et al. (2006).

(1994). The calculated temperatures for this assemblage vary from 515 to 593±75 °C, at 0 kbar, and 481 to 547±75 °C, at 5 kbar.

Temperature and pressure conditions of the sodic–calcic alteration were also estimated using an internally consistent thermodynamic database (TWQ software; Berman, 1991), considering albite, actinolite/magnesiohornblende, titanite, epidote, quartz, and calcite in equilibrium. P–X_{CO_2} and T–X_{CO_2} were used to evaluate X_{CO_2} conditions. Equilibrium conditions for this assemblage were estimated to be approximately 1.4 kbar and 500 °C (Fig. 16), at X_{H_2O}=0.6 and X_{CO_2}=0.4.

6.2. Chloritization

Chlorite is a common mineral phase in mineralized veins and breccias. In the Sequeirinho orebody, chlorite is mainly related to actinolite alteration in mineralized breccias. In the Sossego orebodies, chlorite replaces biotite in potassic alteration zones (Fig. 10A, B) and actinolite and epidote in the matrix of mineralized breccias, where it commonly occurs associated with quartz, epidote and calcite (Fig. 10C–F). This latter assemblage could suggest its formation through the reaction below (Cho and Liou, 1987; Laird, 1988):

$$\text{Epidote} + \text{Actinolite} + H_2O + CO_2 = \text{Calcite} + \text{Chlorite} + \text{Quartz}.$$

This reaction occurs at subgreenschist facies temperatures in the presence of CO_2, consuming actinolite and epidote. Stability fields for calcite–epidote–chlorite–quartz and calcite–epidote–quartz assemblages are also restricted to lower temperature than those typical of the lower greenschist facies, although this association could be stable at relatively higher temperature at high X_{CO_2}.

The geothermometer based on $Al^{(IV)}$ contents of chlorite of Cathelineau and Nieva (1985) was applied using composition of chlorite from mineralized breccias of the Sequeirinho and Sossego orebodies. As correlation between $Al^{(IV)}$ and Fe/(Fe+Mg) was verified for chlorite from the Sossego orebody, correction for the $Al^{(IV)}$–T dependency using Fe/(Fe+Mg) ratios of the Sossego chlorite was adopted, as proposed by Kranidiotis and MacLean (1987), Jowett (1991), and Zang and Fyfe (1995). The calculated temperatures vary from 160 and 210 °C (Sossego orebody) and 230 to 280 °C (Sequeirinho orebody).

7. Discussion

7.1. The Sossego hydrothermal system evolution

The Sossego hydrothermal system displays a complex alteration and mineralization sequence characterized by early sodic, sodic–calcic, potassic, chloritic, calcic, and hydrolytic alteration zones. This alteration sequence is in general accordance with the "classical" system of alteration zoning predicted in IOCG systems (Hitzman et al., 1992; Haynes, 2000). The Cu–Au mineralization occurs late in the hydrothermal alteration sequence, which is also the case in other IOCG systems, e.g., Candelária, Chile (Marschik and Fontboté 2001), Tjårrojåkka, Sweden (Edfelt et al., 2005) and Ernest Henry, Australia (Mark et al., 2006), where Cu–Au mineralization postdates the main iron oxide stage.

Conditions estimated indicated temperatures exceeding 550 °C during the early sodic–calcic alteration stage at Sequeirinho (TQW method and the geothermometer of Holland and Blundy, 1994), and markedly lower temperatures (<300 °C) for the paragenetically later Cu–Au mineralization in both orebodies. These conditions are in general agreement with those estimated using oxygen stable isotopes (Monteiro et al., 2008). However, in the case of the Sossego mineralization stage, the estimated temperature values (210 to 160 °C) are lower than those calculated using isotopic compositions of mineral pairs from the mineralization stage (302 °C; quartz–calcite and 253 °C; calcite–apatite; Monteiro et al., 2008). These temperatures possibly are very low for the ore stage. Conditions for potassic alteration were not estimated, but the paragenetic evolution at Sossego suggests intermediate conditions between those calculated for sodic–calcic alteration (>550 °C) and chloritization (<300 °C). Calculations using actinolite and magnesiohornblende compositions from the Sequeirinho sodic–calcic alteration zones indicated pressure conditions of ~1.5 kbar, implying evolution of the main hydrothermal activity at shallow crust levels.

7.2. Amplibole chemistry: comparison with Carajás IOCG deposits

Amphibole from ore breccias in both orebodies has similar compositions and similar zoned patterns, which may reflect temperature decreases during the ore stage associated with episodic hydrothermal fluid pulses. This could explain the decrease of Fe^{2+} content in the Sossego actinolite and the oscillatory variations in the Sequeirinho amphibole.

Comparison of hydrothermal amphibole compositions in the Sossego deposit and those from other IOCG deposits in the Carajás Mineral Province, such as Igarapé Bahia (Dreher, 2004; Gomes and Lindenmayer, 2003), Salobo, and Gameleira (Gomes and Lindenmayer, 2003) indicates the common occurrence of at least two co-existing amphibole types in all these deposits (Fig. 17).

The composition of these two types of amphibole may be grouped as:

(i) Amphibole with $(Na+K)_A$ contents higher than 0.5, high chlorine (up to 3.77% at Sequeirinho, 1.96% at Gameleira, and 1.57% in Salobo amphibole), and high Al^{IV} and Fe/(Fe+Mg) ratios. It is

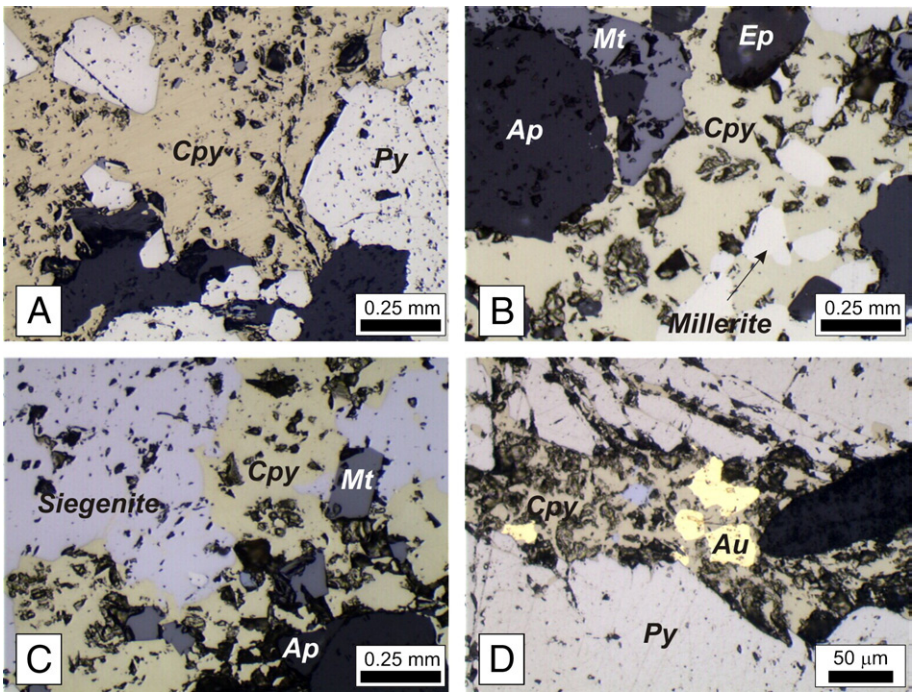

Fig. 14. Photomicrography of ore breccias in the Sequeirinho and Sossego orebodies (reflected light). (A) Chalcopyrite and pyrite from ore breccia from Sequeirinho; inclusion of gold in chalcopyrite; (B) late millerite associated with chalcopyrite in Sequeirinho breccia. Chalcopyrite involves early crystallized apatite, magnetite, and epidote; (C) siegenite associated with chalcopyrite and euhedral magnetite in Sossego breccia; (D) gold occurs associated with chalcopyrite, that infills fractures in early pyrite in Sossego breccia. Abbreviations: Ap = apatite; Cpy = chalcopyrite; Ep = epidote; Mt = magnetite; Py = pyrite.

ferro-edenite, hastingsite, pargasite or ferro-pargasite (Fig. 17) with the variation controlled by edenitic exchange mechanisms.

(ii) Amphibole with $(Na+K)_A$ contents less than 0.5 and with the composition of actinolite, ferro-actinolite, ferro-hornblende, magnesiohornblende, tschermakite, and ferrotschermakite controlled mainly by ferritschermakitic and subordinate edenitic exchange mechanisms.

The Fe/(Fe+Mg) ratios in amphibole from IOCG deposits in the Carajás Province are variable (Fig. 17). The lowest Fe/(Fe+Mg) ratios are those reported for amphibole from sodic–calcic alteration and mineralized zones of the Sequeirinho (0.15 to 0.60) and mineralized veins and breccias of the Sossego (0.29 to 0.51) orebodies. Amphibole from restricted haloes close to contact between gabbro and granite in the Sequeirinho orebody has higher Fe/(Fe+Mg) ratios, between 0.51 and 0.63, which are within the range observed for Gameleira and Salobo amphibole (0.57 to 0.82 and 0.41 to 0.75, respectively). The Igarapé Bahia amphibole, however, has the highest Fe/(Fe+Mg) ratios (0.71 to 1.00).

Negative correlation between #Mg and Cl contents (Fig. 17) indicates that Mg–Cl avoidance mechanisms could control the halogen incorporation in amphibole structure. Correlation between Cl and K or (Na+K)A contents are also present in these amphiboles (Fig. 17). This correlation is typical of amphibole crystallized in Cl-rich environment (Hanley and Mungall, 2003), and could indicate that edenitic exchange mechanisms also control Cl incorporation in amphibole. This would be possible because A-site exchange may increase the unit cell volume and the cavity size filled by OH (Enami et al., 1992). As chlorine has a larger ionic ratio, this mechanism favors chlorine incorporation.

The common presence of at least two amphibole types, one of them chlorine-rich, in all IOCG deposits in the Carajás Province, could result from coupled substitution mechanisms that introduce mineral compositional variations from a common chlorine-rich fluid, in a

Table 6
Minor and trace elements (ppm) in sulfides from the Sossego orebody of the Sossego IOCG deposit

	Pyrite				Chalcopyrite				Millerite		Siegenite	
	Sossego		Sequeirinho		Sossego		Sequeirinho		Sossego		Sossego	
	Min	Max	Min	Max	Min	Max	Min	Max	Min	Max	Min	Max
As	<200	1300	<200	1050	<200	670	<200	820	<200	450	<200	<200
Ag	<200	<200	<200	260	<200	290	<200	390	<200	330	<200	<200
Sb	<200	290	<200	450	<200	<200	<200	330	<200	890	<200	<200
Co	4580	22,760	13,200	19,730	<200	<200	<200	460	4810	5130	*	*
Se	<200	5000	<200	4530	<200	2500	<200	1870	<200	<200	<200	5600
Zn	<200	810	<200	1740	<200	460	<200	320	<200	<200	< 200	950
Ni	<200	1810	<200	1790	<200	<200	<200	230	*	*	*	*
Cu	<200	1350	<200	1980	*	*	*	*	<200	1580	2140	10,780
Fe	*	*	*	*	*	*	*	*	4210	10,610	5120	87,530
Pd	<200	<200	<200	<200	<200	<200	<200	<200	<200	1130	<200	530
Te	<200	<200	<200	<200	<200	<200	<200	190	<200	830	<200	<200
Th	<200	<200	<200	<200	<200	570	<200	200	<200	<200	<200	<200

* = major element.

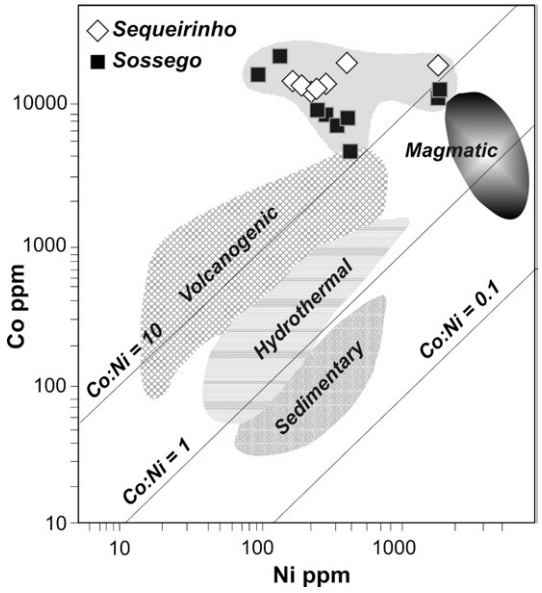

Fig. 15. Variations of Ni and Co contents in pyrite from the Sossego and Sequeirinho orebodies and fields for pyrite composition from Bajwah et al. (1987), Brill (1989) and Xu (1998).

similar way to that reported by Coulson et al. (2001). Alternatively, however, the amphibole composition could reflect an evolving hydrothermal system with preferential chlorine incorporation during early sodic–calcic episodes.

7.3. Halogen contents in the hydrothermal fluid, metal transport and mechanisms of ore deposition

Chlorine-bearing mineral phases have been previously described in other IOCG deposits of the Carajás Mineral Province, such as the Igarapé Bahia (Zang and Fyfe, 1995; Tavaza et al., 1999; Dreher, 2004), Salobo (Guimarães, 1987), Gameleira (Lindenmayer et al., 2001), Pojuca Corpo Quatro (Winter, 1994), and Cristalino (Huhn et al., 1999) deposits.

In addition to the evidence that Sequeirinho amphibole from rocks in contact with gabbros was crystallized in a Cl-rich environment, chlorine [IV(Cl)] and chlorine/fluorine intercepts [IV(Cl/F)] calculated from biotite composition (Munoz, 1984) also indicate that the hydrothermal fluids associated with potassic alteration at Sossego were significantly chlorine-enriched.

Estimated log (fH_2O)/($fHCl$) values (2.5 to 3.0; Table 3) using equations of Zhu and Sverjenski (1992), at 500 °C, are similar to those calculated for IOCG deposits (2.8 to 3.6) from the Mt Isa Block, Australia (Marshall and Oliver, 2006), but lower than those typical of porphyry-Cu deposits (3.5 to 5.5; Selby and Nesbitt, 2000), at similar temperatures. This could imply in fluids with higher HCl fugacity in the Sossego deposit and other IOCG deposits than those associated with porphyry-Cu deposits.

If lower exchange temperatures (<500 °C) are considered for Sossego biotite, similar fluids in terms of HCl fugacity might be related with these different systems (Fig. 11). However, as thermodynamic calculations indicate that high temperatures facilitate Cl substitution for OH^- in biotite (Zhu et al., 1994), significantly lower exchange temperatures (<400 °C) could be unreasonable. Thus, the halogen chemistry might reflect differences in the fluids involved in these hydrothermal systems.

The abundance and speciation of fluorine and chlorine in aqueous fluids is of broad interest in the study of ore deposits because of the potential role these ligands may play in the complexing and hence transport of Au, Cu and other metals (e.g., Enami et al., 1992; Baker, 1998; Mazdab and Barton, 2001; Coulson et al., 2001; Hanley and Mungall, 2003). The halogen content in hydrous silicates has been studied mainly in porphyry-Cu and intrusion-related Au-systems (Munoz, 1984; Selby and Nesbitt, 2000; Coulson et al., 2001), where chlorine-rich aqueous solutions, derived from immiscibility processes or from evolution of magmas crystallized at low pressures, are considered responsible for extraction of large amounts of Cu from magma (Candela and Holland, 1986; Candela, 1989). The presence of chlorine-rich hydrous silicate is also typical of iron oxide Cu–Au deposits (Mazdab and Barton, 2001), but the relationship between halogen contents and magmatic fluid evolution is controversial for these deposits (Barton and Johnson, 1996, 2000; Pollard, 2001, 2006).

An important role of an evaporite component is considered in many IOCG systems, which could involve more saline, Cl-rich and S-poor fluids than those generated from magmas (Barton and Johnson, 1996, 2000; Frietsch et al., 1997; Hitzman, 2000; Ullrich et al., 2001; Mazdab and Barton, 2001). Other authors (Pollard, 2001, 2006; Perring et al., 2001) have emphasized the importance of unmixing of CO_2-rich magmatic fluids to generate a hypersaline aqueous phase responsible for the extraction of large quantities of Cu from magma.

At Sossego, oxygen and hydrogen isotope studies result in ambiguous evidence of magmatic fluid participation in the ore genesis (Monteiro et al., 2008), however $\delta^{37}Cl$ values (0 to 2.1‰) and associated Cl/Br ratios indicate participation of magmatic mantle-derived fluids and basinal brines in the Sossego IOCG system (Chiaradia et al., 2006). Boron isotopic signatures in tourmaline from the Sossego deposit (−8 to +11‰) are also attributed to mixed sources, including leaching from igneous rocks and marine evaporites (Xavier et al., 2005).

Irrespective of their origin, high-temperature, Cl-rich highly saline fluids were probably responsible by transport of metals as metal chloride complexes in the Sossego hydrothermal system. Intermediate-oxidation (magnetite stable) conditions were estimated from biotite composition for the potassic alteration stage. Hypersaline, neutral to weakly acidic and intermediate-reduced brines, similar to those related with potassic alteration (Fig. 18), can transport thousands of ppm of Cu at 400 °C (Liu and McPhail, 2005). Gold is also highly soluble at high temperature (>350 °C) and/or high Cl^- concentration (Henley, 1973). Ore deposition in this evolving system

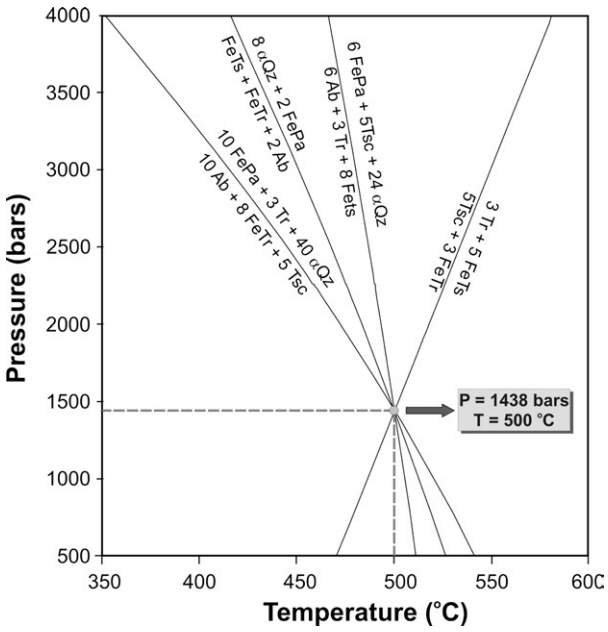

Fig. 16. TQW thermobarometry for the sodic–calcic alteration assemblage with actinolite/magnesiohornblende–albite–epidote–quartz–calcite–titanite of the Sequeirinho orebody. Mineral abbreviations after Kretz (1983). End-member activities from Berman (1988), McMullin et al. (1991), Mader and Berman (1992), and Fuhrman and Lindsley (1988).

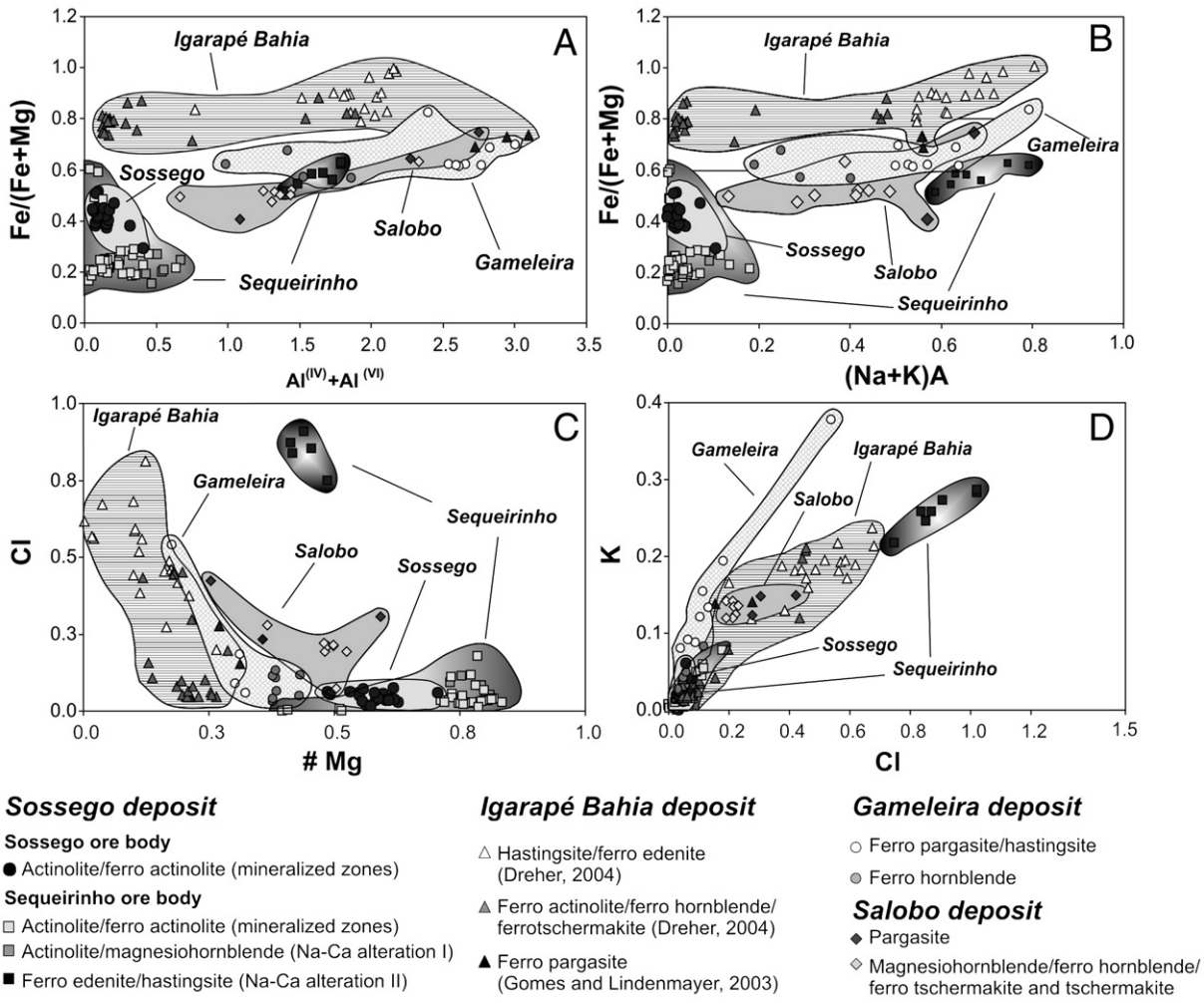

Fig. 17. A. $Al^{IV}+Al^{VI}$ *vs.* Fe/(Fe+Mg); B. $(Na+K)_A$ *vs.* Fe/(Fe+Mg); C. #Mg *vs.* Cl; and D. Cl *vs.* K_A diagrams showing the composition of amphibole from IOCG deposits of the Carajás Mineral Province. Data sources: Sossego deposit (this work); Igarapé Bahia: Dreher (2004), Gomes and Lindenmayer (2003); Gameleira and Salobo: Gomes and Lindenmayer (2003).

would require reduced salinities of the fluid and/or temperature decrease.

Decrease of chlorine contents of the fluid might have been achieved either by fluid mixing or by loss of chlorine to minerals, as evidenced by chlorine incorporation in amphibole, biotite, apatite, and scapolite. Reduced temperatures in the ore stage are recorded by mineral chemistry and stable isotope compositions (Monteiro et al., 2008) of gangue minerals. This could be a function of time as well as favored by the influx of cooler and more diluted meteoric fluids into the system, possibly associated with episodic decompression due to fluid overpressure. This is suggested by the oxygen isotope signatures for fluids in equilibrium with syn-ore minerals (quartz, calcite, epidote, chlorite) from both orebodies ($\delta^{18}O_{H_2O}=-1.8\pm3.4‰$; Monteiro et al., 2008).

Although different mechanisms may have triggered metal deposition in the Sossego hydrothermal system, fluid mixing between a high-temperature, hypersaline, intermediate-oxidation state, metalliferous brine and oxidized meteoric-derived fluids is considered to have been the principal ore deposition mechanism. This mixing process was responsible for a trend (Fig. 18) from high-temperature relatively reduced to low-temperature oxidized conditions in the late stages of the system evolution.

7.4. Magnetite–Cu–Au–Co–Ni–Pd–REE association

In the Carajás Mineral Province, the common association between Co and Ni with IOCG deposits has been related to underplating of mafic magma during the rift development associated with the Carajás Basin installation, which could have contaminated later magmatic pulses (Tallarico et al., 2005). Cobalt, Ni, and PGE enrichments have been also recognized as an important characteristic of the IOCG deposits elsewhere (Mazdab and Force, 1998; Mazdab and Barton, 2001; Sillitoe, 2003).

The association between Ni–Co enrichment and mafic rocks have been documented in Eloise (Baker, 1998) and Mt. Elliot (Wang and Williams, 2001) IOCG deposits, Cloncurry district, Australia, Candelária, Punta del Cobre, Manto Verde, and Cerro Negro IOCG deposits in Chile and Peru (Sillitoe, 2003), and in the Variscan Iberian Massif (Tornos and Casquet, 2005). Sm–Nd isotopic studies in the Olympic Dam IOCG deposit, Australia, indicate that the ore signature is not derived only from the host granite, but might result from contribution from mantle-derived magma or rocks, such as mafic–ultramafic dikes that occur in the area (Johnson and McCulloch, 1995).

According to Sillitoe (2003), a linkage of central Andean IOCG deposits to oxidized dioritic magmas may be compared with the well-documented dependency of several other magmatic-hydrothermal deposit types on igneous petrochemistry. However, the association between Co-bearing sulfides and chlorine-rich silicates, contrasts with the environment typical of magmatic-hydrothermal systems in which magmatic brines typically results from immiscibility of felsic magmas (Mazdab et al., 1999; Mazdab and Barton, 2001). This could be more compatible with a metal source from mafic igneous rocks rather than from magmas.

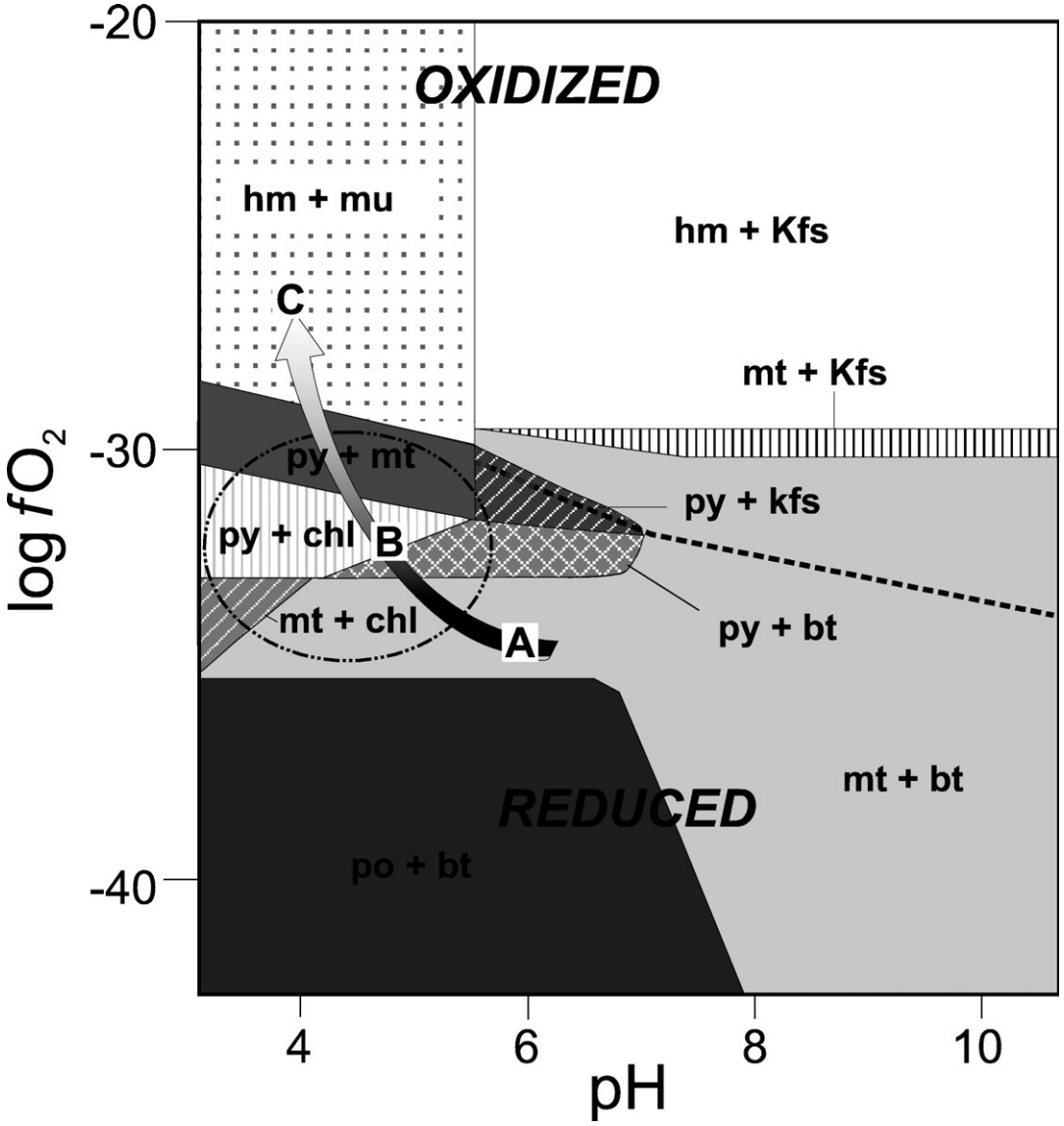

Fig. 18. Oxygen fugacity and pH conditions, at 300 °C, 1.5 kbar, aK+ = 0.1 (Skirrow, 2004), for potassic alteration (A), main mineralization stage (B), and hydrolytic assemblage. Dashed field represents predominant conditions during the ore stage at Sossego.

Electron-microprobe studies in the Sossego deposit point to significant enrichments in Co, Ni, Pd and Se, associated with REE, Th and U in the ore zones. Cassiterite inclusions in chalcopyrite are also very common together with Ni-, Co-, and Pd-bearing mineral phases. This geochemical signature possibly reflects the chemistry of the host rocks leached by hydrothermal fluids. Metal leaching from the host rocks was probably enhanced by the high chlorine contents of the hydrothermal fluids in the extensive hydrothermal systems driven by heat from several intrusive episodes recorded in the Carajás Mineral Province.

In the Sossego deposit, gabbro bodies, which have close spatial relationship with massive magnetite bodies and mineralized zones, could represent a possible source for Co and Ni. These gabbros are probably related with the 2.65 to 2.70 Ga gabbro dikes and sills (Dias et al., 1996; Mougeot et al., 1996) that are widespread in the Carajás Province. Additionally, Co, Ni and Pd might have also been stripped from metaultramafic lenses that occur imbricated within metavolcanic rocks at Sequeirinho and mafic–ultramafic differentiated complexes (e.g., Luanga complex, 2763±6 Ma; Machado et al., 1991) that occur in the Carajás Mineral Province and contain PGE enrichments. Thus, the geochemistry signature of the Carajás IOCG deposits could reflect their genesis within an Archean cratonic block in which plume-induced partial melting of subcontinental lithosphere would be also responsible for PGE-bearing mafic–ultramafic intrusions (Groves and Bierlein, 2007).

8. Conclusions

The Sossego IOCG deposit comprises two major orebodies, Sequeirinho and Sossego, which have distinct styles of hydrothermal alteration that probably reflect different host rocks, intensity of fluid–rock interactions, and paleostructural levels. Despite the predominance of sodic–calcic alteration at Sequeirinho and potassic alterations and chloritization at Sossego, there is a general similarity in the zoned patterns and chemical composition of syn-ore minerals, and in the ore geochemical signatures (Fe oxide–Cu–Au–Co–Ni–Pd–REE–U) in both orebodies. This could suggest similar fluid evolution and metal sources.

Fluid–rock interaction processes might have resulted in significant metal leaching from the host sequences, favored by both high temperature (>500 °C) of the initial system and high chloride concentration in the hydrothermal fluids. Thus, the ore geochemical

signature possibly reflects the chemistry of the host rocks (gabbro, granite, granophyric granite, and felsic metavolcanic rocks with minor lenses of metaultramafic rocks) leached by hydrothermal fluids.

Estimated conditions for different stages of hydrothermal alteration and mineralization indicate sharp temperature decrease during the system evolution (>500 °C to <300 °C). This reflects fluid–rock interaction and influx of meteoric-derived fluids, which was likely favored by the shallow crustal setting. Temperature decrease, redox changes, chlorine incorporation in hydrothermal minerals, and fluid mixing represent effective mechanisms of ore precipitation. These processes might favor sulfide deposition at low temperatures (<300 °C), associated with a brittle structural environment.

Acknowledgments

We are very grateful to the Companhia Vale do Rio Doce (CVRD) for the continuous support provided to the researchers and students of the Institute of Geosciences-UNICAMP during their activities in the Carajás region. We feel particularly indebted to Márcio Godoy, José Jacob Fanton, Benevides Aires and Roberta Morais for their invaluable orientation in the field. We wish to thank Cesar Fonseca Ferreira Filho and Onésio Rodrigues Nunes Filho (Universidade de Brasília — UnB), John Skok (Colorado School of Mines), and Dailto Silva and Rosane Palissari (IG-UNICAMP) who assisted with the electron-microprobe and scanning electronic microscopy studies. We would like also to thank the anonymous reviewers and Dr. Nigel J. Cook, whose critical comments and suggestions significantly improved the paper. This research has been supported by the Fundação de Amparo à Pesquisa do Estado de São Paulo — FAPESP (Procs. No. 03/01159-1, 04/08126-4, 03-11163-6, 03/09584-3, 03/07453-9), FAPESP/PRONEX 03/09916-6 and FAEP/UNICAMP grants. R.P Xavier and C.R. Souza Filho acknowledge CNPq for research grants 300579/92-6 and 301.227/94, respectively.

References

Araújo, O.J.B., Maia, R.G.N., Jorge-João, X.S., Costa, J.B.S., 1988. A megaestruturação da folha Serra dos Carajás. Congresso Latino Americano de Geologia. Proceedings, vol. 7, pp. 324–333.

Bailey, S.W., 1980. Summary of recommendations of AIPEA Nomenclature Committee. Clays and Clay Minerals 15, 85–93.

Bajwah, Z.U., Secombe, P.K., Offler, R., 1987. Trace element distribution, Co:Ni ratios and genesis of the Big Cadia iron–copper deposit, New South Wales, Australia. Mineralium Deposita 22, 292–300.

Baker, T., 1998. Alteration, mineralization, and fluid evolution at the Eloise Cu–Au deposit, Cloncurry district, northwest Queensland, Australia. Economic Geology 93, 1213–1236.

Barros, C.E.M., Barbey, P., 1998. Auréolas tectônicas: um novo modelo de evolução tectono-metamórfica para a Província Mineral de Carajás. Congresso Brasileiro de Geologia, vol. 40, Anais, Sociedade Brasileira de Geologia, p. 53.

Barros, C.E.M., Sardinha, A.S., Barbosa, J.P.O., Krimski, R., Macambira, M.J.B., 2001. Pb–Pb and U–Pb zircon ages of Archean syntectonic granites of the Carajás metallogenic province, northern Brazil. South American Symposium on Isotopic Geology. Proceedings, vol. 3, pp. 94–97.

Barton, M.D., Johnson, D.A., 1996. Evaporitic source model for igneous-related Fe oxide–(REE–Cu–Au–U) mineralization. Geology 24, 259–262.

Barton, M.D., Johnson, D.A., 2000. Alternative brine sources for Fe-oxide(–Cu–Au) systems: implications for hydrothermal alteration and metals. In: Porter, T.M. (Ed.), Hydrothermal Iron Oxide Cooper–Gold and Related Deposits: a Global Perspective. Australian Mineral Foundation, vol.1. Adelaide, pp. 43–60.

Beaudoin, G., Gosselin, P., Dupois, C., Jébrak, M. 2006. La composition des oxydes de fer: un nouvel outil d'exploration. Québec Exploration 2006. http://www.quebecexploration.qc.ca/pdf/session1_10h50_beaudoingeorges.pdf.

Berman, R.G., 1988. Internally-consistent thermodynamic data for stoichiometric minerals in the system Na_2O–K_2O–CaO–MgO–FeO–Fe_2O_3–Al_2O_3–SiO_2–TiO_2–H_2O–CO_2. Journal of Petrology 29, 445–522.

Berman, R.G., 1991. Thermobarometry using multiequilibrium calculations: a new technique with petrologic applications. Canadian Mineralogist 29, 833–855.

Brill, B.A., 1989. Trace-element contents and partitioning of elements in ore minerals from the CSA Cu–Pb–Zn deposit, Australia. Canadian Mineralogist 27, 263–274.

Bryndzia, L.T., Scott, S.D., 1987. The composition of chlorite as a function of sulfur and oxygen fugacity: an experimental study. American Journal of Science 287, 50–76.

Candela, P.A., 1989. Felsic magmas, volatiles, and metallogenesis. Reviews in Economic Geology 4, 223–233.

Candela, P.A., Holland, H.D., 1986. A mass transfer model for copper and molybdenum in magmatic hydrothermal systems: the origin of porphyry-type ore deposits. Economic Geology 81, 1–19.

Carvalho, E.R., Xavier, R.P., Monteiro, L.V.S., Souza Filho, C.R., 2005. Geology and hydrothermal alteration of the Sossego iron oxide–copper–gold deposit, Carajás Mineral Province, Brazil. Simpósio Brasileiro de Metalogenia, 1, [CD-ROM].

Cathelineau, M., Nieva, D., 1985. A chlorite solid solution geothermometer: the Los Azufres (Mexico) geothermal system. Contributions to Mineralogy and Petrology 91, 235–244.

Chiaradia, M., Banks, D., Cliff, R., Marschik, R., de Haller, A., 2006. Origin of fluids in iron oxide–copper–gold deposits: constraints from δ^{37}Cl, $^{87}Sr/^{86}Sr$ and Cl/Br. Mineralium Deposita 41, 565–573.

Cho, M., Liou, J.G., 1987. Phrenite–pumpellyte to greenschist facies transition in the Karmutsen metabasites, Vancouver Island, B.C. Journal of Petrology 28, 417–443.

Coulson, I.M., Dipple, G.M., Raudsepp, M., 2001. Evolution of HF and HCl activity in magmatic volatiles of the gold-mineralized Emerald Lake pluton, Yukon Territory, Canada. Mineralium Deposita 36, 594–606.

Dall'Agnol, R., Costi, H.T., Leite, A.A., Magalhães, M.S., Teixeira, N.P., 1999. Rapakivi granites from Brazil and adjacent areas. Precambrian Research 95, 9–39.

Dall'Agnol, R., Lafon, J.M., Macambira, M.J.B., 1994. Proterozoic anorogenic magmatism in the Central Amazonian Province, Amazonian Craton: geochronological, petrological and geochemical aspects. Mineralogy and Petrology 50, 113–118.

Dall'Agnol, R., Souza, Z.S., Althoff, F.J., Barros, C.E.M., Leite, A.A.S., Jorge-João, X.S., 1997. General aspects of the granitogenesis of the Carajás metallogenetic province. International Symposium on Granites and Associated Mineralizations. Salvador, Excursion Guide, vol. 2, pp. 135–161.

Dardenne, M.A., Schobbenhaus, C.S., 2001. Metalogênese do Brasil. Editora Universidade de Brasília/CNPq, Brasília. 392 pp.

De Bruyin, H., Van der Westhuized, W.A., Schoch, A.E., 1983. The estimation of FeO, F and H_2O^+ by regression in microprobe analyses of natural biotite. Journal of Trace and Microprobe Techniques 1 (4), 399–413.

De Jong, G., Williams, P.J., 1995. Giant metasomatic system formed during exhumation of mid-crustal Proterozoic rocks in the vicinity of the Cloncurry Fault, northwest Queensland. Australian Journal of Earth Sciences 42, 281–290.

Dias, G.S., Macambira, M.B., Dall'Ágnol, R., Soares, A.D.V., Barros, C.E.M., 1996. Datações de zircões de sill de metagabro: comprovação de idade arqueana da Formação Águas Claras, Carajás, Pará. Simpósio de Geologia da Amazônia, vol. 5, pp. 376–378. Extended Abstracts, SBG.

Docegeo, 1988. Revisão litoestratigráfica da Província Mineral de Carajás – Litoestratigrafia e principais depósitos minerais. Congresso Brasileiro de Geologia. Belém, SBG, Anexo aos anais, vol. 35, pp. 11–54.

Dreher, A.M., 2004. O depósito primário de Cu–Au de igarapé Bahia, Carajás: Rochas fragmentárias, fluidos mineralizantes e modelo metalogenético. Ph.D. Thesis, Univesidade Estadual de Campinas, 221pp.

Edfelt, Å., Armstrong, R.N., Smith, M., Martinsson, O., 2005. Alteration paragenesis and mineral chemistry of the Tjårrojåkka apatite–iron and Cu (–Au) occurrences, Kiruna area, northern Sweden. Mineralium Deposita 40, 409–434.

Enami, M., Liou, J.G., Bird, D.K., 1992. Cl-bearing amphibole in the Salton Sea geothermal system, California. Canadian Mineralogist 30, 1077–1092.

Faraco, M.T.L., Carvalho, J.M.A., Klein, E.L., 1996. Carta metalogenética da Província Carajás-SE do estado do Pará, Folha Araguaia (SB-22). Nota explicativa. CPRM, Belém.

Frietsch, R., Tuisku, P., Martinsson, O., Perdahl, J.A., 1997. Early Proterozoic Cu–(Au) and Fe ore deposits associated with regional Na–Cl metasomatism in northern Fennoscandia. Ore Geology Reviews 12, 1–34.

Fuhrman, M.L., Lindsley, D.H., 1988. Ternary-feldspar modeling and thermometry. American Mineralogist 73, 201–216.

Galarza, M.A., Macambira, M.J.B., 2002a. Geocronologia e Evolução Crustal da Área do Depósito de Cu–Au Gameleira, Província Mineral de Carajás (Pará), Brasil. Geologia USP Série Científica 2, 143–159.

Galarza, M.A., Macambira, M.J.B., 2002b. Petrologia e geocronologia das rochas encaixantes do depósito de Cu–Au Igarapé Bahia, Província Mineral de Carajás, Pará, Brasil. In: Kein, E.L., Vasquez, M.L., Rosa-Costa, L.T. (Eds.), Contribuições à geologia da Amazônia, vol. 3. SBG/NN, Belém, pp. 153–168.

Gomes, C.H., Lindenmayer, Z.G., 2003. Anfibólios cálcicos dos depósitos de Cu–Au de Gameleira, Salobo e Bahia, Província Mineral de Carajás, Pará: minerais metamórficos ou hidrotermais?, In: Ronchi, L.H., Althoff, F.J. (Eds.), Caracterização e modelamento de depósitos minerais, 1 ed. São Leopoldo - RS, v. 1, pp. 119–145.

Gosselin, P., Beaudoin, G., Jébrak, M., 2006. Application of the geochemical signature of iron oxides to mineral exploration. GAC-MAC Annual Meeting Program with Abstracts [CD-ROM].

Gow, P.A., Wall, V.J., Oliver, N.H.S., Valenta, R.K., 1994. Proterozoic iron oxide (Cu–U–Au–REE) deposits: further evidence of hydrothermal origins. Geology 22, 633–636.

Groves, D.I., Bierlein, F.K., 2007. Geodynamic settings of mineral deposit systems. Journal of the Geological Society (London) 164, 19–30.

Guimarães, I.G., 1987. Petrologia da formação ferrífera na área Salobo 3a - Província Mineral de Carajás, PA. Dissertação de Mestrado, Instituto de Geociências, Universidade de São Paulo, São Paulo. 99 pp.

Hanley, J.J., Mungall, J.E., 2003. Chlorine enrichment and hydrous alteration of the Sudbury Breccia hosting footwall Cu–Ni–PGE mineralization at the Fraser Mine, Sudbury, Ontario, Canada. The Canadian Mineralogist 41, 857–881.

Haynes, D.W., 2000. Iron oxide copper(–gold) deposits: their position in the ore deposit spectrum and modes of origin. In: Porter, T.M. (Ed.), Hydrothermal Iron Oxide Cooper–Gold and Related Deposits: a Global Perspective. Australian Mineral Foundation, vol. 1. Adelaide, pp. 71–90.

Haynes, D.W., Cross, K.C., Bills, R.T., Reed, M.H., 1995. Olympic Dam ore genesis: a fluid-mixing model. Economic Geology 90, 281–307.

Henley, R.W., 1973. Some fluid dynamics and ore genesis. Transactions Institution of Mining and Metallurgy 82, B1–B8.
Hitzman, M.W., 2000. Iron oxide–Cu–Au deposits: what, where, when, and why. In: Porter, T.M. (Ed.), Hydrothermal Iron Oxide Cooper–Gold and Related Deposits: a Global Perspective. Australian Mineral Foundation, vol.1. Adelaide, pp. 9–25.
Hitzman, M.W., Oreskes, N., Einaudi, M.T., 1992. Geological characteristics and tectonic setting of Proterozoic iron oxide (Cu–U–Au–REE) deposits. Precambrian Research 58, 241–287.
Holland, T., Blundy, J. 1995. Software: HbPl 1.2. (ftp://http://www.esc.cam.ac.uk/pub/minp/HB-PLAG/).
Holland, T., Blundy, J., 1994. Non-ideal interactions in calcic amphiboles and their bearing on amphibole–plagioclase thermometry. Contributions to Mineralogy and Petrology 116, 443–447.
Huhn, S.R.B., Santos, A.B.S., Amaral, A.F., Ledsham, E.J., Gouveia, J.L., Martins, L.P.B., Montalvão, R.M.G., Costa, V.C., 1988. O terreno granito-greenstone da região de Rio Maria – Sul do Pará. Congresso Brasileiro de Geologia, vol. 35, Anais, Sociedade Brasileira de Geologia, p. 1438–1452.
Huhn, S.R.B., Soares, A.D.V., Souza, C.I.J., Albuquerque, M.A.C., Leal, E.D., Vieira, E.A.P., Masotti, F.S., Brustolin, V., 2000. The Cristalino copper–gold deposit, Serra dos Carajás, Pará. International Geological Congress, 31, Rio de Janeiro, IUGS, [CD-ROM].
Huhn, S.R.B., Souza, C.I.J., Albuquerque, M.C., Leal, E.D., Brustolin, V., 1999. Descoberta do depósito Cu(Au) Cristalino: Geologia e mineralização associada região da Serra do Rabo - Carajás - PA. Simpósio de Geologia da Amazônia, vol. 6. Sociedade Brasileira de Geologia/Núcleo Norte, pp. 140–143.
Hunt, J., Baker, T., Thorkelson, D., 2005. Regional-scale Proterozoic IOCG-mineralized breccia systems: examples from the Wernecke Mountains, Yukon, Canada. Mineralium Deposita 40, 492–514.
Johnson, J.P., McCulloch, M.T., 1995. Sources of mineralising fluids for the Olympic Dam deposit (South Australia): Sm–Nd isotopic constraints. Chemical Geology 121, 177–199.
Jowett, E.C., 1991. Fitting iron and magnesium into the hydrothermal chlorite geothermometer. GAC/MAC/SEG Join Annual Meeting, Program with Abstract, vol. 16, p. A62.
Juliani, C., 2000. Software: Twq File Archivist 1.0.
Kranidiotis, P., MacLean, W.H., 1987. Systematics of chlorite alteration at the Phelps Dodge massive sulfide deposit, Matagami, Quebec. Economic Geology 82, 1888–1911.
Kretz, R., 1983. Symbols for rock-forming minerals. American Mineralogist 68, 277–279.
Laird, J., 1988. Chlorites: metamorphic petrology. In: Bailey, S.W. (Ed.), Hydrous Phyllosilicates (Exclusive of Micas). Reviews in Mineralogy, 19, pp. 405–454.
Lancaster, Oliveira, J., Fanton, J., Almeida, A.J., Leveille, R.A., Vieira, S., 2000. Discovery and geology of the Sossego copper–gold deposit, Carajás District, Pará State, Brazil. International Geological Congress, 31, Rio de Janeiro, IUGS, [CD-ROM].
Leake, B.E., Woolley, A.R., Arps, C.E.S., Birch, W.D., Gilbert, M.C., Grice, G.D., Hawthorne, F.C., Kato, A., Kisch, H.J., Krivovichev, V.G., Linthout, K., Laird, J., Mandarino, J., Maresch, W.V., Nickel, E.H., Rock, N.M.S., Shumacher, J.C., Smith, D.C., Stephenson, N.C.N., Ungaretti, L., Wittaker, E.J.W., Youzhi, G., 1997. Nomenclature of amphiboles. Report of Subcommittee on Amphiboles of the International Mineralogical Association Commission on New Minerals and Mineral Names. European Journal of Mineralogy 9, 623–651.
Lindenmayer, Z.G., Pimentel, M.M., Ronchi, L.H., Althoff, F.J., Laux, J.H., Araújo, J.C., Fleck, A., Bortowski, D.C., Nowatzki, A.C., 2001. Geologia do depósito de Cu–Au do Gameleira, Serra dos Carajás, Pará. In: Jost, H., Brod, J.A., Quieroz, E.T. (Eds.), Caracterizacão de Depósitos Auríferos Brasileiros, ADIMB–DNPM, Brasília, pp. 79–139.
Liu, W., McPhail, D.C., 2005. Thermodynamic properties of copper chloride complexes and copper transport in magmatic-hydrothermal solutions. Chemical Geology 221, 21–39.
Macambira, J.B., Macambira, M.J.B., Scheller, T., Gomes, A.C.B., 1996. Geocronologia Pb/Pb e tipologia de zircões de rochas vulcânicas da Formação Carajás-Pará: indicador da idade dos BIFs. Congresso Brasileiro de Geologia. Boletim de Resumos Expandidos, vol. 39, pp. 516–518.
Machado, N., Lindenmayer, D.H., Krough, T.E., Lindenmayer, Z.G., 1991. U–Pb geochronology of Archean magmatism and basement reactivation in the Carajás area, Amazon Shield, Brazil. Precambrian Research 49, 1–26.
Mader, U.K., Berman, R.G., 1992. Amphibole thermobarometry: a thermodynamic approach. Current Research, Part E. Geological Survey of Canada 92-1E, 393–400.
Mark, G., Oliver, N.H., Williams, P.J., 2006. Mineralogical and chemical evolution of the Ernest Henry Fe oxide–Cu–Au ore system, Cloncurry district, northwest Queensland, Australia. Mineralium Deposita 40, 769–801.
Marschik, R., Fontboté, L., 2001. The Candelaria-Punta del Cobre Iron Oxide Cu–Au (–Zn–Ag) deposits, Chile. Economic Geology 96, 1799–1826.
Marshall, L.J., Oliver, N.H.S., 2006. Monitoring fluid chemistry in iron oxide–copper–gold-related metasomatic processes, eastern Mt Isa Block, Australia. Geofluids 6, 45–66.
Mazdab, F.K., Barton, M.D., 2001. Distinctive chlorine and trace element contents in silicates and sulfides from metasomatic iron-oxide systems. Geological Society of America, Abstracts with Programs 33, 32.
Mazdab, F.K., Force, E.R., 1998. Comparison of cobalt and nickel contents in sulfides from iron-oxide–(Cu–Au–U–REE) occurrences with other hydrothermal and magmatic systems. Geological Society of America, Abstracts with Programs 30 (7), 369.
Mazdab, F.K., Barton, M.D., Hervig, R.L., 1999. Trace element distribution in iron sulfides and associated oxides, with a focus on Fe-oxide-rich hydrothermal systems. Geological Society of America, Abstracts with Programs 31 (7), 32.
McMullin, D., Berman, R.G., Greenwood, H.J., 1991. Calibration of the SGAM thermobarometer for pelitic rocks using data from phase equilibrium experiments and natural assemblages. Canadian Mineralogist 29, 889–908.
Monteiro, L.V.S., Xavier, R.P., Hitzman, M.W., Johnson, C.A., Carvalho, E.R., Souza Filho, C.R., Torresi, I., 2008. Spatial and temporal zoning of hydrothermal alteration and mineralization in the Sossego iron oxide–copper–gold deposit, Carajás Mineral Province, Brazil: paragenesis and stable isotope constraints. Mineralium Deposita 43, 129–159. doi:10.1007/s00126-006-0121-3.
Monteiro, L.V.S., Xavier, R.P., Johnson, C.A., Hitzman, M.W., Carvalho, E.R., Souza Filho, C.R., 2005. The Sossego iron oxide–copper–gold deposit, Carajás Mineral Province, Brazil: stable isotope constraints on the genesis and hydrothermal system evolution. In: Simpósio Brasileiro de Metalogenia, 1, Gramado, Short Papers [CD-ROM].
Morais, R.P.S., Alkmim, F.F., 2005. O controle litoestrutural da mineralização de cobre do Depósito Sequeirinho, Canaã dos Carajás, PA. In: Simpósio Brasileiro de Metalogenia, 1, Gramado, Short Papers [CD-ROM].
Mougeot, R., Respaut, J.P., Briqueu, L., Ledru, P., Milesi, J.P., Lerouge, C., Marcoux, E., Huhn, S.B., Macambira, M.J.B., 1996. Isotope geochemistry constraints for Cu, Au mineralizations and evolution of the Carajás Province (Para, Brazil). Congresso Brasileiro de Geologia, 39, Boletim de Resumos Expandidos, Sociedade Brasileira de Geologia, vol. 7, pp. 321–324.
Munoz, J.L., 1984. F–OH and Cl–OH exchange in micas with applications to hydrothermal ore deposits. In: Bailey, S.W. (Ed.), Micas. Reviews in Mineralogy, vol. 13, pp. 469–493.
Munoz, J.L., 1992. Calculation of HF and HCl fugacities from biotite compositions; revised equations. Geological Society of America, Abstracts with Programs 24, 221.
Nogueira, A.C.R., 1985. Análise faciológica e aspectos estruturais da Formação Águas Claras, região central da Serra dos Carajás. M.Sc. Thesis, Universidade Federal do Pará, 168 pp.
Perring, C.S., Pollard, P.J., Dong, G., Nunn, A.J., Blake, K.L., 2001. The Lightning Creek sill complex, Cloncurry District, Northwest Queensland, a source of fluids for Fe oxide Cu–Au mineralization and sodic–calcic alteration. Economic Geology 95, 1067–1089.
Pidgeon, R.T., Macambira, M.J.B., Lafon, J.M., 2000. Th–U–Pb isotopic systems and internal structures of complex zircons from an enderbite from the Pium Complex, Carajás Province, Brazil: evidence for the ages of granulite facies metamorphism and the protolith of the enderbite. Chemical Geology 166, 159–171.
Pimentel, M.M., Lindenmayer, Z.G., Laux, J.H., Armstrong, R., Araújo, J.C., 2003. Geochronology and Nd geochemistry of the Gameleira Cu–Au deposit, Serra dos Carajás, Brazil: 1.8–1.7 Ga hydrothermal alteration and mineralization. Journal of South American Earth Sciences 15, 803–813.
Pimentel, M.M., Machado, N., 1994. Geocronologia U–Pb dos terrenos granito-greenstone de Rio Maria, Pará. Congresso Brasileiro de Geologia, vol. 38, Anais, Sociedade Brasileira de Geologia, p. 390–391.
Pinheiro, R.V.L., Holdsworth, R.E., 1997. Reactivation of Archaean strike-slip fault systems, Amazon region, Brazil. Journal of the Geological Society of London 154, 99–103.
Pollard, P.J., 2001. Sodic–(calcic) alteration in Fe-oxide–Cu–Au districts: an origin via unmixing of magmatic H_2O–CO_2–NaCl+$CaCl_2$–KCl fluids. Mineralium Deposita 36, 93–100.
Pollard, P.J., 2006. An intrusion-related origin for Cu–Au mineralization in iron oxide–copper–gold (IOCG) provinces. Mineralium Deposita 41, 179–187.
Reche, J., Martinez, F.J., 1996. GPT: an Excel spreadsheet for thermobarometric calculations in metapelitic rocks. Computers and Geosciences 22, 775–784.
Richard, L.R., 1997. Minpet Geological Software Version 2.02 — Mineralogical and Petrological Data Processing System.
Rigon, J.C., Munaro, P., Santos, L.A., Nascimento, J.A.S., Barreira, C.F. (2000) Alvo 118 copper–gold deposit — geology and mineralization, Serra dos Carajás, Para, Brazil. 31st International Geological Congress, Abstract volume [CD-ROM].
Rodrigues, E.S., Lafon, J.M., Scheller, T., 1992. Geocronologia Pb–Pb da Província Mineral de Carajás: primeiros resultados. Congresso Brasileiro de Geologia, vol. 37, Boletim de Resumos Expandidos. Sociedade Brasileira de Geologia, vol. 2, pp. 183–184.
Rotherham, J.F., Blake, K.L., Cartwright, I., Williams, P.J., 1998. Stable isotope evidence for the origin of the Mesoproterozoic Starra Au–Cu deposit, Cloncurry District, Northwest Queensland. Economic Geology 93, 1435–1449.
Selby, D., Nesbitt, B.E., 2000. Chemical composition of biotite from the Casino porphyry Cu–Au–Mo mineralization, Yukon, Canada: evaluation of magmatic and hydrothermal fluid chemistry. Chemical Geology 171, 77–93.
Sillitoe, R.H., 2003. Iron oxide–copper–gold deposits: an Andean view. Mineralium Deposita 38, 787–812.
Skirrow, R., 2004. Iron oxide Cu–Au deposits: an Australian perspective on their unifying characteristics. In: McPhie, J., McGoldrick, P. (Eds.), Dynamic Earth: Past, Present and Future. Abstracts of the 17th Australian Geological Convention, February 8–13th, Hobart, Tasmania. Geological Society of Australia, p. 121. 2004 Abstracts No. 73.
Souza, L.H., Vieira, E.A.P., 2000. Salobo 3 Alpha deposit: geology and mineralization. In: Porter, T.M. (Ed.), Hydrothermal Iron Oxide Copper–Gold and Related Deposits: a Global Perspective. Australian Mineral Foundation, vol. 1. Adelaide, pp. 203–212.
Souza, S.R.B., Macambira, M.J.B., Scheller, T., 1996. Novos dados geocronológicos para os granitos deformados do rio Itacaiúnas (Serra dos Carajás, Pará): implicações estratigráficas. Simpósio de Geologia da Amazônia. Boletim de Resumos Expandidos, Sociedade Brasileira de Geologia/Núcleo Norte, vol. 5, pp. 380–383.
Tallarico, F.H.B., Figueiredo, B.R., Groves, D.I., Kositcin, N., McNaughton, N.J., Fletcher, I.R., Rego, J.L., 2005. Geology and SHRIMP U–Pb geochronology of the Igarape Bahia Deposit, Carajás copper–gold belt, Brazil, an Archean (2.57 Ga) example of iron-oxide Cu–Au–(U–REE) mineralization. Economic Geology 100, 7–28.
Tallarico, F.H.B., McNaughton, N.J., Groves, D.I., Fletcher, I.R., Figueiredo, B.R., Carvalho, J.B., Rego, J.L., Nunes, A.R., 2004. Geological and SHRIMP II U–Pb constraints on the age and origin of the Breves Cu–Au–(W–Bi–Sn) deposit, Carajás, Brazil. Mineralium Deposita 39, 68–86.

Tavaza, E., Oliveira, C.G., Gomes, N.S., 1999. Ocorrência de ferrospirosmalita nas brechas mineralizadas do depósito de Au–Cu–(±ETR-U) de Igarapé Bahia, Província Mineral de Carajás. Revista Brasileira de Geociências 29, 345–348.

Tornos, F., Casquet, C., 2005. A new scenario for related IOCG and Ni–(Cu) mineralization: the relationship with giant mid-crustal mafic sills, Variscan Iberian Massif. Terra Nova 17, 236–241.

Trendall, A.F., Basei, M.A.S., De Laeter, J.R., Nelson, D.R., 1998. SHRIMP U–Pb constraints on the age of the Carajás formation, Grão Pará Group, Amazon Craton. Journal of South American Earth Sciences 11, 265–277.

Ullrich, T., Clark, A.H., Kyser, T.K., 2001. The Candelaria Cu–Au deposit, III Region, Chile, product of long-term mixing of magmatic-hydrothermal and evaporite-sourced fluids. Geological Society of America, Abstracts with Programs 33 (6), 3.

Villas, R.N., Santos, M.D., 2001. Gold deposits of the Carajás Mineral Province: deposit types and metallogenesis. Mineralium Deposita 36, 300–331.

Villas, R.N., Lima, L.F.O., Neves, M.P., Sousa, F.D.S., Lamarão, C.N., Fanton, J., Morais, R. 2005. Relações entre deformação, alteração hidrotermal e mineralização no depósito Cu–Au do Sossego, Província Mineral de Carajás. In: Simpósio Brasileiro de Metalogenia, 1, [CD-ROM].

Wang, S., Williams, P.J., 2001. Geochemistry and origin of Proterozoic skarns at the Mount Elliot Cu–Au–(–Co–Ni) deposit, Cloncurry district, NW Queensland, Australia. Mineralium Deposita 36, 109–124.

Winter, C., 1994. Geology and base-metal mineralization associated with Archean iron-formation in the Pojuca Corpo Quatro deposit, Carajás, Brazil. Ph.D. Thesis, University of Southampton, U.K., 300 pp.

Wirth, K.R., Gibbs, A.K., Olszewski Jr., W.J., 1986. U–Pb ages of zircons from the Grão Pará Group and Serra dos Carajás granite, Pará, Brasil. Revista Brasileira de Geociências 16, 195–200.

Wones, D.R., Eugster, H.P., 1965. Stability of biotite: experiment, theory and application. American Mineralogist 50, 1228–1272.

Xavier, R.P., Wiedenbeck, M., Dreher, A.M., Rhede, D., Monteiro, L.V.S., Araújo, C.E.G., 2005. Chemical and boron isotopic composition of tourmaline from Archean and Paleoproterozoic Cu–Au deposits in the Carajás Mineral Province. Brazilian Symposium on Metallogeny, 1, [CD-ROM].

Xu, G., 1998. Geochemistry of sulfide minerals at Dugald River, NW Queensland, with reference to ore genesis. Mineralogy and Petrology 63, 119–139.

Zang, W., Fyfe, W.S., 1995. Chloritization of the hydrothermally altered bedrock at the Igarapé Bahia gold deposit, Carajás, Brazil. Mineralium Deposita 30, 30–38.

Zhu, C., Sverjensky, D.A., 1992. F–Cl–OH partitioning between biotite and apatite. Geochimica et Cosmochimica Acta 56, 3435–3467.

Zhu, C., Xu, H., Ilton, E.S., Veblen, D.R., Henry, D.J., Tivey, M.K., Thompson, G., 1994. TEM–AEM observations of Cl-rich amphibole and biotite and possible petrologic implications. American Mineralogist 79, 909–920.